MC REPORT 109

THE FACT MODEL

VOLUME I

C. W. Spofford

November 1974

ACOUSTIC ENVIRONMENTAL SUPPORT DETACHMENT

OCEAN SCIENCE PROGRAM
MAURY CENTER FOR OCEAN SCIENCE
Department of the Navy
Washington, D.C.

SECURITY CLASSIFICATION OF THIS PAGE (When Data Entered)

REPORT DOCUMENTATION PAGE

READ INSTRUCTIONS BEFORE COMPLETING FORM

1. REPORT NUMBER: MAURY CENTER REPORT 109
2. GOVT ACCESSION NO.
3. RECIPIENT'S CATALOG NUMBER

4. TITLE (and Subtitle): (6) THE FACT MODEL . Volume I,
5. TYPE OF REPORT & PERIOD COVERED
6. PERFORMING ORG. REPORT NUMBER

7. AUTHOR(s): (10) C. W. SPOFFORD
8. CONTRACT OR GRANT NUMBER(s)

9. PERFORMING ORGANIZATION NAME AND ADDRESS:
ACOUSTIC ENVIRONMENTAL SUPPORT DETACHMENT
OFFICE OF NAVAL RESEARCH
ARLINGTON, VIRGINIA 22217
10. PROGRAM ELEMENT, PROJECT, TASK AREA & WORK UNIT NUMBERS: PE63795

11. CONTROLLING OFFICE NAME AND ADDRESS:
ACOUSTIC ENVIRONMENTAL SUPPORT DETACHMENT
OFFICE OF NAVAL RESEARCH
ARLINGTON, VIRGINIA 22217
(11) Nov 74
12. REPORT DATE: NOVEMBER 1974
13. NUMBER OF PAGES: 77

14. MONITORING AGENCY NAME & ADDRESS (if different from Controlling Office)
(12) 76
15. SECURITY CLASS. (of this report): UNCLASSIFIED
15a. DECLASSIFICATION/DOWNGRADING SCHEDULE

16. DISTRIBUTION STATEMENT (of this Report)

UNLIMITED DISTRIBUTION

(14) MC-109-VOL-1

17. DISTRIBUTION STATEMENT (of the abstract entered in Block 20, if different from Report)

18. SUPPLEMENTARY NOTES

19. KEY WORDS (Continue on reverse side if necessary and identify by block number)

TRANSMISSION LOSS
ACOUSTICS MODEL
FACT

404 409

20. ABSTRACT (Continue on reverse side if necessary and identify by block number)

The FACT (Fast Asymptotic Coherent Transmission) Model is the new Navy Interim Standard Transmission Model for ocean environments which may be treated within the context of a single sound-speed profile and a flat bottom. It is a ray-acoustics model designed for the computation of transmission loss as a function of range and frequency at fixed depth. The classical ray treatment has been augmented with higher order asymptotic

(OVER)

corrections in the vicinity of caustics, and the phased addition of selected paths experiencing significant, predictable coherence effects. The computer program is fully automated requiring only the specification of the environment and the essential parameters.

This report consists of two volumes, the first describing the physics and mathematics contained in the FACT model as well as comparisons of FACT and normal-mode results, the second describing the program structure and flow with complete samples of input and output. Volume I is being distributed to a broad community of both technical and application-oriented users as a Maury Center Report. Volume II is intended primarily for programmers attempting to implement the model on their computers and has been distributed as an AESD Technical Note only to recipients of the FACT program. Volume II as well as the complete program listing and punched-card deck will be provided by AESD to qualified users upon request.

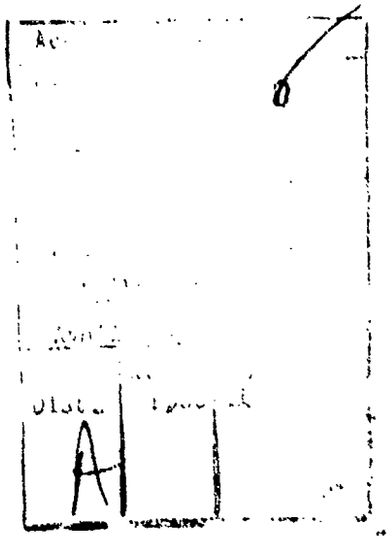

PREFACE

In April 1973, the FACT model was designated as the Navy Interim Standard Model for the prediction of transmission loss in an environment which can be characterized by a flat bottom and a single sound speed profile. At that time, preliminary documentation was distributed to Navy laboratories and other qualified users.

These volumes contain a detailed description of the physics, mathematics, and computer implementation of the FACT program. Questions concerning the model or suggestions for its improvements should be addressed to the Acoustic Environmental Support Detachment of the Office of Naval Research.

J. B. Hersey

J. B. HERSEY

TABLE OF CONTENTS

LIST OF ILLUSTRATIONS

LIST OF ILLUSTRATIONS (Continued)

LIST OF ACRONYMS

Abbreviation	Definition
AESD	Acoustic Environmental Support Detachment
ASRAP	Acoustic Sensor Range Prediction
BTL	Bell Telephone Laboratories
FACT	Fast Asymptotic Coherent Transmission
FNWC	Fleet Numerical Weather Central
LRAPP	Long Range Acoustic Propagation Project
NOO	Naval Oceanographic Office
NUC	Naval Undersea Center
RBR	Refracted-Bottom Reflected
RP70	Ray-tracing Program (1970)
RR	Refracted-Refracted
RSR	Refracted (at depth) -Surface Reflected
SRBR	Surface Reflected-Bottom Reflected
SUDS	Surface Duct Sonar
WKB	Wentzel-Kramers-Brillouin

GLOSSARY OF TERMS

TERM	DEFINITION
Arrival	When a ray traced from the source of rays crosses the receiver depth.
Arrival Order	Set of arrivals of all rays which have the same number of deep reversals (refracted at depth or bottom reflected).
Asymptotic	Converging to the exact result in the high-frequency limit.
Caustic	Envelope of a family of rays; a smooth caustic may develop a cusp at certain points.
Coherent	Adding path amplitudes on a phased basis.
Convergence zone	Region of focusing or convergence of rays.
False caustic	Caustic which is an artifact of the linearly segmented sound-speed profile.
Half channel	Sound-speed profile increasing monotonically from surface to bottom; usually, though not necessarily, isothermal.

GLOSSARY OF TERMS (Continued)

TERM	DEFINITION
Incoherent	Adding path intensities without phase.
Layered medium	Sound speed varies only with depth, and water depth is independent of range.
Leakage	Loss of energy from a surface duct to the main sound channel (analogous to quantum-mechanical tunneling through a potential barrier).
Low-frequency cut-off	Frequency below which no trapped normal mode may exist for a given channel or duct.
Ray class	Set of rays distinguished by their having the same histories at their reversals or turning points (i.e. RR, RSR, SRBR, RBR).
Ray family	Subset of rays of the same class which are processed together to compute arrivel intensities. for a given arrival order of a family the range of arrival may be assumed to be a continuous smooth function of ray angle.

GLOSSARY OF TERMS (Continued)

TERM	DEFINITION
Ray-equivalent	The "ray-equivalent" of the m-th normal mode for a given sound-speed satisfies the relation: $\oint k_z dz = 2\pi m + \delta\phi$ where k_z is the vertical wave number of the ray ($k_z = 2\pi f \sin\theta / c(z)$), the integral is taken over the full ray cycle, and $\delta\phi$ corresponds to the discrete phase shifts accumulated by the ray (π at surface reflections, $\pi/2$ at caustics).
Reciprocity	Fact that ray paths and ray amplitudes are independent of the direction of propagation (permits interchange of source and receiver).
rms	Root mean square or incoherent summation of paths.
Semi-coherent	Adding ray paths on a partially coherent basis when the degree of coherence is governed by the resolution of the resulting interference pattern as specified by the range sampling.

GLOSSARY OF TERMS (Continued)

TERM	DEFINITION
Surface-image interference	Interference pattern observed between the direct and surface-reflected pair of paths for shallow source or receiver depths.

1.0 INTRODUCTION AND BACKGROUND

On April 1, 1973, the Acoustic Environmental Modeling Coordinator, Dr. J. B. Hersey, designated a new Navy Interim Standard Transmission Model (FACT - Fast Asymptotic Coherent Transmission) for ocean environments which may be treated within the context of a single sound-speed profile and a flat bottom. This model resulted from a three-year effort in acoustic modeling sponsored by the Long Range Acoustic Propagation Project (LRAPP) within several Navy and industrial laboratories. As a part of this program LRAPP hosted in March 1971 a workshop on acoustic modeling by ray-tracing techniques. Sixteen different organizations active in the field of ray tracing participated, and a by-product of the workshop was a "consensus model" consisting of components drawn from several models. Subsequent to the workshop Bell Telephone Laboratories (BTL) developed for LRAPP a special purpose program based upon this consensus model and oriented specifically to the Airborne Sensor Range Prediction (ASRAP) program at Fleet Numerical Weather Central (FNWC , Monterey, Cal.) where speed was crucial. In October 1972, a preliminary version of this model was turned over to AESD which in turn delivered to FNWC on March 15 a fully automated upgraded model. For a typical deep-water ASRAP case the transmission loss is computed every 0.5 nm to 125 nm at four frequencies for each pair of source and receiver depths in 4 to 8 seconds.

While the FACT model was originally designed for ASRAP, it is sufficiently general for many other applications. Since turning it over to FNWC, AESD has distributed it to 37 other Navy and industrial activities in six different countries. The documentation of this model has to date

consisted of four BTL publications (Spofford, 1972a, 1972b, 1972c and 1973a) and descriptive material generated by AESD and included as part of a fully annotated listing. This report represents the final technical documentation of the FACT model as of 1 December 1973. As with any computer representation of a complex physics problem substantive modifications and improvements in the physics are likely, as are some bugs in the code which have eluded initial testing. The FACT model has been extensively tested and is run several hundred times daily by FNWC. As bugs are uncovered, however, AESD will provide correction sets to all users. In addition, when any improvements in physics are made, technical addenda to this report will be issued.

The FACT model is a ray-acoustics model designed for the computation of transmission loss as a function of range and frequency at fixed source and receiver depths. The classical ray treatment has been augmented with higher order asymptotic corrections and the phased addition of selected paths. These improvements yield a more complete model of diffraction and coherence effects, respectively, found to be important in long-range low-frequency propagation. The basic physics package has been fully automated so that the only inputs required are the specification of the environment and the parameters of the case desired. While programs incorporating more precise ray tracing may exist (involving curvilinear sound speed profiles, ray targeting, etc.), none appears to contain as complete and automated a treatment of the diffraction and coherence effects so important at low frequencies. The program has been constructed in an extremely modular form which should accomodate both the incorporation of new physics packages as well as the needs of the R&D community for a

flexible basic framework within which new theories and techniques may be investigated.

This report consists of four basic sections in two volumes:

Volume I

1. A summary of the capabilities of the FACT model, its strengths and weaknesses, and those areas in which future improvements are planned as part of a detailed description of the physics represented by the program. Examples are provided comparing normal-mode computations and FACT output to illustrate several of its novel features.

2. A description of the mathematical implementation of the model with all relevant equations.

Volume II [Provided routinely to all recipients of the FACT Program, available upon request, and taken nearly verbatim from a report issued by Ocean Data Systems, Inc., documenting the FACT program (Baker, 1973)]

1. A description of the program structure and the program flow including readable flow charts of all routines.

2. A copy of the original FACT documentation prepared by AESD and normally included with a full program listing ("FACT Handout"). This documentation included samples of the complete input and output for three test cases to assist new users in implementing and debugging the program on their computers. The full program listing has not been included

in this report. Upon request [illegible] a FACT listing and a punched-card deck are avail[illegible]

1.1 Acknowledgments

This program was developed in its original form by the author while at Bell Telephone Laboratories. The initial idea for such a program resulted from discussions with Captain W. S. Houston, Commanding Officer FNWC, Monterey. Its development at BTL was encouraged by Drs. J. A. Polak and U. F. Gianola and supported under contract N00014-69-C-0088 by the Long Range Acoustic Propagation Project of the Office of Naval Research. Its implementation at FNWC and ultimate adoption as a Navy Standard Model would not have been possible without the enthusiastic support of CDR P. R. Tatro and LCDR T. J. McCloskey of LRAPP, and Mr. J. R. Clark of FNWC.

The advances in propagation modeling contained in the program represent the research efforts of several people. Mr. M. A. Pedersen's work at the Naval Undersea Center (NUC) on false caustics and convergence-zone ranging formed the basis for the intensity-processing algorithms and demonstrated the applicability of the Brekhovskikh caustic corrections. Three of the author's co-workers at BTL deserve special recognition for their contributions to propagation modeling: **Dr. F. M. Labianca** for recognizing the applicability to underwater propagation of Ludwig's uniform treatment of caustics; Dr. R. L. Holford for applying Ludwig's work to the analysis of three- and four-ray systems; and Dr. J. S. Hanna for demonstrating the importance of long-range surface-image interference. Several useful discussions with Dr. J. B. Hersey (ONR) during the preparation of this report are greatfully acknowledged.

Finally, the author is especially indebted to Mr. C. L. Baker of Ocean Data Systems, Incorporated, who upgraded the original computer code to a product with considerably fewer bugs and in a form which is sufficiently modular to be useful to a wide community. Mr. Baker converted a program written by scientists and engineers into a computer program, and is entirely responsible for the more lucid portions of the FACT code.

2.0 SUMMARY OF BASIC CAPABILITIES OF THE FACT MODEL

This section is intended to familiarize the reader with the basic capabilities and limitations of FACT, in terms of the physical model it represents. A discussion is also included of those areas of the program which will be improved and extended in the future. It should be re-emphasized that the modularity of the program will permit modelers to test new theories and approaches quite easily using the basic FACT framework. The discussion in this section has been divided into two major parts addressing:

1. The model used for the ocean environment;

2. The ray treatment of this environment.

2.1 The Ocean Environment

The model used for the ocean environment is "layered"; that is, neither the sound-speed profile nor the bottom depth are range dependent. The sound-speed profile, $c(z)$, is approximated by a continuous piecewise-linear function of depth z, so that within each layer the sound-speed gradient, $c'\left(=\frac{dc}{dz}\right)$, is a constant and at layer boundaries c' is discontinuous. (The effects of such discontinuities have been well studied (Pedersen, 1961) and will be addressed in sections 3.1 and 3.2.) Within the water column a frequency-dependent volume attenuation (or absorption) is included of the form

$$\alpha = \begin{cases} 2f^2\left[\frac{.1}{1+f^2} + \frac{40}{4100+f^2}\right] & f>1 \\ .125\ f^2 & f<1 \end{cases} \qquad (2\text{-}1)$$

where f is the frequency in kilohertz and α is a loss in dB per nautical mile. This expression corresponds to Thorp's absorption (Thorp, 1965) above 1 kHz and is an empirical result derived by FNWC (Parka I, 1969) below 1 kHz.

The ocean bottom is modeled as a reflecting surface where each ray suffers a reflection loss which is dependent upon grazing angle, frequency, and bottom class. The loss suffered as a function of these parameters is given by the FNWC bottom-loss tables (Bassett and Wolff, 1970) for frequencies less than 1 kHz or greater than 3.1 kHz, and by the new Naval Oceanographic Office (NOO) Navy Standard curves from 1 kHz to 3.5 kHz (Christensen, Frank and Kaufman, 1972).

The ocean surface is modeled as a perfect reflector (with a 180-degree phase shift) for all rays considered. For propagation in a surface duct rays are not used and the surface-duct module (to be described subsequently) includes a rough-surface loss which is dependent on frequency, sea state and mixed layer depth (i.e. duct thickness).

In the three areas of volume absorption, bottom reflectivity, and rough-surface loss improvements are expected. The volume absorption is currently added to the total transmission loss as a function of horizontal range. Ideally volume absorption should be computed on a ray-by-ray basis using the arc length of the ray for the appropriate distance. It is expected that this more accurate computation may be available in the near future, though it will increase the

running time somewhat. More significantly, the low-frequency absorption will be updated as soon as the R&D community agrees on appropriate values applicable to individual ray paths. A more consistent merger of the FNWC and NOO bottom-loss types is needed as well as considerably more data on low-frequency reflectivity. Similarly a good surface-reflectivity model (dependent presumably on grazing angle, frequency, and some measure of surface roughness) is needed, again directly applicable to the coherent, specular scatter of individual rays.

2.2 The Basic FACT Model

This section contains a qualitative description of the basic physics in the FACT model - that is: what effects it does and does not treat; what the relative levels of accuracy of the various approximations employed are; and where treatments might be extended or refined in the future. The detailed discussion of how these computations are performed (equations, approximations, algorithms, etc.) are reserved for Section 3.

Acoustic propagation in the ocean is governed by the wave equation. Ray tracing is a convenient and powerful technique for approximating the exact wave solution. The traditional ray solutions determine all relevant ray paths connecting the source and receiver and sum the geometric intensities of these paths to obtain the total transmission loss. This traditional approach is already an approximation to rigorous ray theory which requires the phased sum of the ray amplitudes. The justification for this approximation is that the phased sum oscillates quite rapidly with range, and

that uncertainties in the geometry and environment preclude an accurate estimate of phase. Hence the phased sum is replaced by the rms sum as an average over the uncertainities in position and environment. As will be shown subsequently, in many significant cases this rms sum is not representative of these or any other meaningful averages.

A second area where traditional ray tracing requires improvements is in the computation of individual ray intensities. According to classical ray theory the intensity of a ray (or, more appropriately, a ray bundle) is inversely proportional to the geometric spreading or divergence of the bundle. In the ocean environment focal points and surfaces occur where the ray divergence is zero and infinite ray intensities are predicted, usually accompanied by immediately adjacent areas of zero intensity (i.e. no rays). The acoustic field associated with these focusing regions, or caustics, is improperly modeled by classical ray theory. The error at low frequencies may be substantial over large regions.

Recent advances in ray theory and the analysis of acoustic measurements have permitted these two major deficiencies of classical ray theory to be overcome. The FACT-model treatment of these improvements as well as algorithms for approximating low-frequency cut-off effects and axis-to-axis propagation are described in the following subsections.

2.2.1 Coherent Summation of Paths

At even very low frequencies, the coherent summation of all ray paths produces very rapid oscillations in the

transmission loss as a function of range. For most applications these oscillations are too rapid to be useful in detail and should be smoothed. Also uncertainties in the environment are sufficient to preclude the prediction of the precise position of these peaks and nulls. What is needed then is a range-averaging technique which smooths these rapid fluctuations while preserving long-term significant departures from the rms sum of all paths.

The long-term departures from the rms sum are primarily due to long-range surface-image interference effects. Figure 2-1 illustrates a typical pair of RSR paths which differ only in the vicinity of the source. The phase difference between these paths consists of the travel-time difference and a phase reversal of π for the path with the additional surface reflection. For shallow sources and low frequencies this phase difference changes quite slowly with range and may, over entire convergence zones, change by considerably less than 1 full cycle (DeAngelis and Spofford, 1970 and Hanna, 1970). Hence the phased sum of these two paths may potentially differ by a uniform amount from the rms sum over significant range intervals.

Fortunately the phase difference may be estimated quite accurately from the ray geometry in the immediate vicinity of the source and detailed travel-time calculations are not necessary. Since the two ray amplitudes are essentially equal a rapidly computed, local phased sum may be obtained. This approach has been incorporated into the FACT model.

Figures 2-2, 2-3, 2-4 and 2-5 compare predictions for an RSR convergence zone using FACT ("RAY THEORY") with an exact normal-mode result for frequencies of 25, 50, 100 and 200 Hz respectively. (The leading edge of this convergence zone contains a caustic which will be discussed subsequently.) The shallow source experiences very strong surface-image interference. As the frequency increases the net effect shifts from uniform near cancellation at 25 Hz to uniform enhancement at 50 and 100 Hz. At 200 Hz the first null in the Lloyd's Mirror interference pattern occurs at 33 miles and is predicted fairly accurately by FACT. It should be noted that the more rapid oscillations in these mode predictions are being intentionally smoothed by FACT.

In addition to either this fully coherent combination of the two paths or the incoherent rms sum, a third "semi-coherent" option is available. The FACT program computes transmission loss at discrete range points, and for deeper sources and/or higher frequencies than those of Figures 2-2, 2-3, 2-4 and 2-5, the interference pattern may be undersampled yielding an apparently random structure. Since the range step is indicative of the amount of detail usually desired in a prediction, the semi-coherent option provides an automated, smooth transition from the fully coherent two-path sum to the incoherent sum as the number of range points per cycle of interference decreases from 6 to $2^2/_3$. This option is recommended for general use, keeping in mind, however, that it may yield range-step dependent transmission loss. Figure 2-6 illustrates the smoothing process in the first bottom-bounce region for varying sampling rates. Finally, these coherence effects are possible at both source and receiver if the receiver is sufficiently shallow, and

where appropriate are included at one or both ends of the ray path.

2.2.2 Caustic Processing

There are three types of focusing regions which are treated by FACT: smooth caustics, cusped caustics, and combined smooth/cusped caustics. The treatments of the first two are based upon thorough analyses of the ray geometries, and the errors associated with any approximations are known. The third case has not been thoroughly analyzed, and the errors associated with its treatment are less well defined.

2.2.2.1 Smooth Caustics (Two-Ray Systems)

Figure 2-7 depicts a family of rays in a simple pressure-gradient profile which form a smooth caustic after the first surface reflection. The caustic is the envelope of this family of rays and forms the classical boundary between the illuminated region (with two rays through each point) and the shadow zone (with no rays present). The classical field increases in the illuminated region to infinity on the caustic surface and is zero in the shadow zone. The actual field as given by wave theory reaches a finite maximum value just inside the illuminated region and decays exponentially into the shadow zone. The key questions left unresolved by classical ray theory are the values of this peak amplitude and the rate of decay (which at low frequencies may be quite gradual).

Higher order asymptotic estimates for these quantities may be obtained (Brekhovskikh, 1960a, Sachs and Silbiger,

1971 and Ludwig, 1966) from the local ray geometry near the caustic. FACT computes these expressions and yields the shadow-zone field, the peak field, and a range average of the very rapid two-ray interference in the illuminated region. The convergence zone comparisons of Figures 2-2, 2-3, 2-4 and 2-5 correspond to the geometry of Figure 2-8, where the receiver ("SOURCE" invoking the usual reciprocity assumptions) is deep and the source is located 50 feet below the surface. At the source depth the caustics of the direct and surface-reflected rays combine on a phased basis and the resulting surface-image interference effects must be included. The primary effect of the caustic corrections in Figures 2-2, 2-3, 2-4 and 2-5 is seen in the increase in slope of the leading edge of the zone as the frequency increases. The changes in peak level with frequency are dominated by coherence effects in this case and do not reflect the weaker frequency dependence of the caustic itself.

At very low frequencies, or for caustics which cross the receiver depth nearly horizontally,* the shadow-zone fall-off is quite slow and, in the approximation of the local caustic geometry, may be computed to extend to great range. Smooth caustics typically originate or terminiate in a cusp (point C in Figure 2-8 which will be discussed in more detail in the following section). Since the shadow-zone field essentially extends no farther than the cusp, FACT tapers the field to be fully decayed at the range of the cusp, preserving its initial behavior at the smooth caustic.

---

* FACT is unable to include the effects of fields associated with caustics which do not reach the receiver (or source) - for example leakage into or out of a surface duct.

2.2.2.2 Cusped Caustics (Three-Ray Systems)

Just as the geometrical acoustics amplitude is invalid at smooth caustics, the smooth-caustic amplitude breaks down at cusped caustics. The cusped caustic C, illustrated in Figure 2-8 occurs where two smooth caustics terminate. Inside the cusp there are three rays through any point and, as with smooth caustics, the field near the cusp may be determined from the local ray geometry (Holford, 1972). An automated computation of the field for general cusped caustics is quite involved; however, the observation that in layered media a cusp always forms at the same depth as the source simplifies the calculation significantly. This case is of particular interest for shallow-source, shallow-receiver geometries (e.g. sonobuoys) and has been accounted for in FACT (averaging over the rapid three-ray interference inside the cusp as in the smooth-caustic interference region).

Figures 2-9, 2-10 and 2-11 compare FACT ("RAY TRACING") with a normal-mode result for the geometry of Figure 2-8 at 25, 50 and 100 Hz respectively. The first cusp occurs at ~21 nm and repeats every 21 nm. Each cusp is preceded at 35, 58 and 80 nm by a smooth caustic which originates at the preceding cusp and is reflected from the surface. For these convergence zones the smooth and cusped caustics are part of the same ray aperture and a potential four-ray system exists. The treatment of such cases is described in the next section.

2.2.2.3 Smooth and Cusped Caustics (Four-Ray Systems)

Figure 2-12 illustrates the canonical cusped-caustic geometry for a shallow source in a warm-water profile. For

a receiver at the source depth the cusp, C, is preceded immediately by a smooth caustic (emanating from the cusp at C'). For more typical, stronger thermocline gradients the separation is considerably less. Also for deeper water than shown in the figure the up-going rays associated with the smooth caustic would penetrate the cusp resulting in four rays through points within the cusp.

In principle, this is a basic four-ray system for which the necessary asymptotic expressions are not available. In practice, the smooth- and cusped-caustic fields may be superimposed to yield reasonable results. For well-separated systems as in Figures 2-9, 2-10 and 2-11 the smooth- and cusped-caustic fields may be added on an rms basis. This is the technique currently incorporated in FACT. For very tight geometries a phased sum of the two fields has been required on occasion (Holford and Spofford, 1972); however, this is a difficult computation to automate. Figures 2-13, 2-14 and 2-15 compare FACT ("RAY TRACING") and normal-mode predictions for a simplified Pacific profile at frequencies of 25, 50 and 100 Hz respectively. The ray geometry is similar to that in Figure 2-12, however, the cusped and smooth caustics are much closer. Only the paths corresponding to the RR rays have been included in the computations except for the FACT predictions from 5 to 30 miles which include bottom-reflected paths. The frequency dependence of the agreement between these predictions suggests that a fully phased combination might yield better agreement. This modification is currently under investigation.

2.2.3 Low-Frequency Cut-Off Effects

In the FACT model the total transmission loss is computed by summing on an incoherent or rms basis the intensities

of sets of rays which contribute to the field at each range/depth point of interest. Within each set (to be described subsequently) certain coherent combinations of paths may have already been performed either explicitly (for surface-image interference) or implicitly (near caustics). The subsequent incoherent combination of these sets assumes that the relative phase differences between sets are both unpredictable and rapidly changing with range. For very low frequencies (geometries with dimensions of several wavelengths) both of these assumptions may be incorrect. Most importantly, as frequencies decrease to near cut-off for the first trapped mode, large-scale cancellations occur resulting in significant uniform degradations from the rms intensity.

In the FACT model this effect is approximated by reducing the amplitudes of rays which would experience uniform destructive interference. The rays expected to experience this interference are those with angles shallower than the ray-equivalent of the first propagating mode as determined by the standard WKB approximations (Brekhovskikh, 1960b). This approach is admittedly approximate and attempts only to capture very gross features. The extension of ray theory to a situation so clearly in the domain of wave techniques is speculative at best. Further study is underway; however, until a thoroughly substantiated technique is developed, wave programs should be used wherever possible for these cases.

2.2.4 Axis-to-Axis Propagation

A persistent problem in ray tracing has been modeling so-called "axis-to-axis" transmission. The difficulty is

illustrated in Figure 2-16 where rays are traced from a source located on the axis of a bilinear profile. At any range on the axis there exists an infinite number (as the ray angle approaches zero) of refracted rays (each of non-zero intensity) connecting the source and receiver. Hence, the rms summation of these paths yields an infinite intensity and the ray solution is invalid. Ignoring low-frequency cut-off effects, this problem is an undesirable by-product of the linearly segmented velocity profile. For profiles with a continuous first derivative of c(z) at the axis (and non-zero second derivative) the near-axial rays focus periodically at cusped caustics along the axis where the focal distance is determined by the second derivative of c(z).

The linearly segmented profile is an approximation to the smoother profile which is usually modeled as having a discontinuous second derivative across the axis. This model simulates the basic asymmetry of the sound-channel axis where the decrease in sound speed associated with the thermocline gradient is overtaken by the increase in sound speed associated with the "pressure gradient". The discontinuous second derivative gives two weak focal points along the axis (F_1 and F_2 in Figure 2-17) between each strong focal point (F_o). All rays about the axis are focussed at F_o, whereas only upgoing and only downgoing rays are focused at F_1 and F_2 respectively.

The motivation for this model for the sound-channel axis is to capture the character of transmission associated with the near-axial rays. The prominent feature of these rays is the strong focus F_o. The implementation of this approach in FACT is accomplished by:

1. Estimating the second derivatives of c(z) above and below the axis and establishing an equivalent smooth profile;

2. Computing the corresponding period (distance to F_o) for the axial ray in the smooth profile;

3. Finding the ray of minimum angle in the linearly segmented profile with this period;

4. If source and receiver are between the upper and lower turning points of this ray, moving both the source and receiver to the depth of either the upper or lower turning point.

The resulting transmission loss for this set of near-axial rays will then exhibit the strong focusing of a cusped caustic (simulating the focusing at F_o) at the appropriate range. By moving the source and receiver to the same depth whenever they are both between the turning points, the gross features of the near-axial wave field are assumed to be essentially independent of depth for a near-axis source.

2.2.5 Modeling Surface-Ducted Propagation

FACT presently contains the same surface-duct module as the Navy Standard Long-Range Transmission Model, RP70. The model was developed for PMWC by Clay and Tatro (Clay, 1968) to characterize the gross features of ducted propagation. The intensity in the surface duct is found from conservation of energy modified by additional losses (proportional to range) caused by duct leakage and rough-surface

scattering of energy from the duct (Marsh and Schulkin, 1967). This basic intensity is independent of source or receiver depth so long as both are in the duct. For cross-duct cases (only one in the duct) the intensity is reduced by 10 dB, and for neither in the duct no ducted contribution is computed.

A preliminary analysis of this model (Labianca, 1972) has shown that the leakage term does not correspond to the mechanism which dominates duct leakage and, in particular, has the wrong dependence on the below-layer (thermocline) gradient. An intensive investigation of all available surface duct models has been completed recently by NUC for LRAPP (Morris, 1974). This study compared several models with each other and the SUDS transmission-loss data (Cummins, 1972). Since none of the candidate models emerged as clearly superior, AESD is currently studying possible modifications to the surface-duct equations.

In the normal operating mode no rays are traced in the surface duct and the intensity associated with ducted paths is computed by the duct module. The user has the option of tracing rays in the duct and computing intensities using the standard FACT algorithms. This procedure is not recommended in general for several reasons:

1. Long-range computations require excessive computer time;

2. No leakage, or surface-scattering effects are included;

3. Cross-layer coupling is not computed.

Nevertheless comparisons of rays versus mode calculations can be informative in cases where the above considerations are not crucial. Such a case is illustrated in Figure 2-18 where transmission losses are compared for a 500-foot surface duct at 300 Hz (Spofford, 1973b). The three predictions were generated using the Clay/Tatro model, FACT tracing rays in the duct, and the NUC surface-duct normal-mode model (Bucker, 1970) (considered to be the exact solution for this case). Since the surface was assumed to be flat, and leakage was not significant to the range shown, the agreement is perhaps not that surprising.

2.2.6 Special-Purpose Shallow-Water Model

While the FACT model was designed for deep-water problems, several of the FNWC ASRAP areas have bottom depths less than 1000 feet. When low-loss bottom classes are specified (i.e. no loss up to some apparent critical angle), a very large number of bottom-bounce paths must be computed with an attendant increase in running time. For these low loss cases an option has been provided which approximates the contributions of the surface-reflected bottom-reflected paths with a rapid computable analytical expression. This expression approximates the summation of all paths by an integral which includes the surface-image interference effects. The resulting transmission-loss curve corresponds to a running range average of the FACT prediction.

2.2.7 Special-Purpose Half-Channel Model

Another case which requires excessive computing time for ASRAP forecasts is "half-channel" transmission; that is,

the case in which the sound speed increases montonically from the surface to the bottom. For shallow sources and receivers in this environment (essentially a very deep surface duct) considerable computer time is consumed in obtaining a transmission loss curve for the RSR paths which is quite smooth (due to the considerable overlap of the arrival orders). In such cases, the water is nearly isothermal, and the key parameters for RSR propagation are the source, receiver, and water depths and the frequency. Hence for the four frequencies and three source-receiver depth combinations used in ASRAP the FACT RSR intensities (excluding volume attenuation) were fitted with functions of the form (A+BLog(D/1000.))/R where A and B depend upon the frequency/source/receiver depth combination in question, D is the water depth, and R the range. A simple lookup table is then used in actual runs and this RSR intensity is added to the direct-path and bottom-bounce contributions which are computed in the usual way. This routine should only be used for precise ASRAP geometries and frequencies since it is not necessarily representative of other cases.

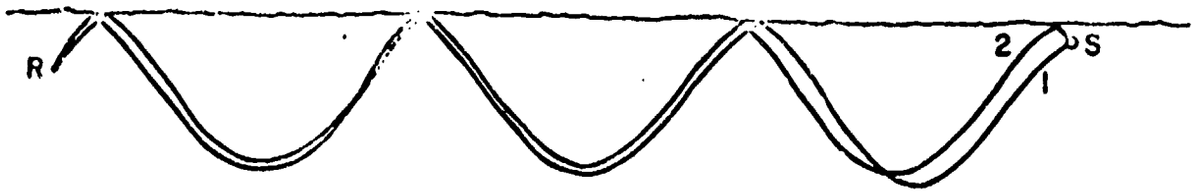

Figure 2-1. Typical Pair of Paths Experiencing Long-Range Surface-Image Interference

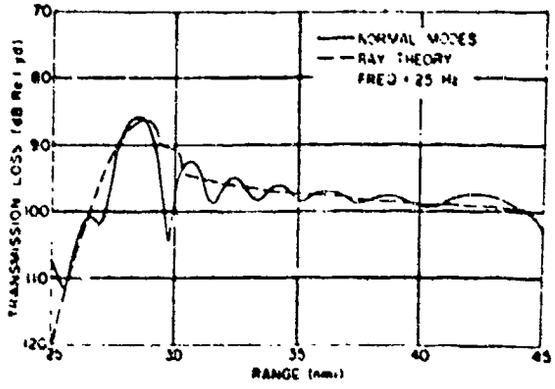

Figure 2-2. 25 Hz

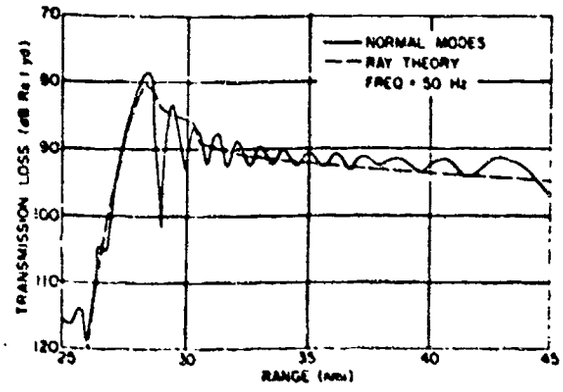

Figure 2-3. 50 Hz

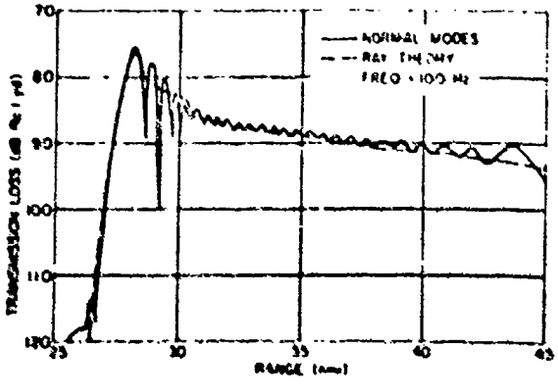

Figure 2-4. 100 Hz

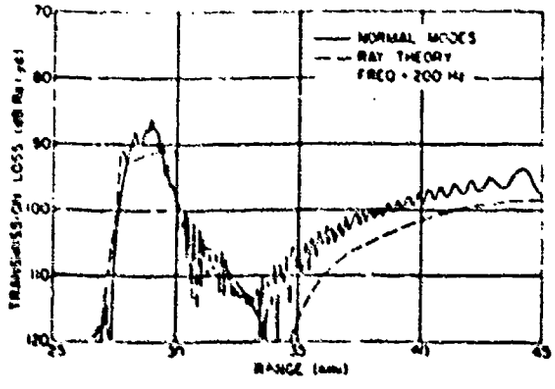

Figure 2-5. 200 Hz

Comparison of FACT ("RAY THEORY") with Normal Modes for an RSR Convergence Zone

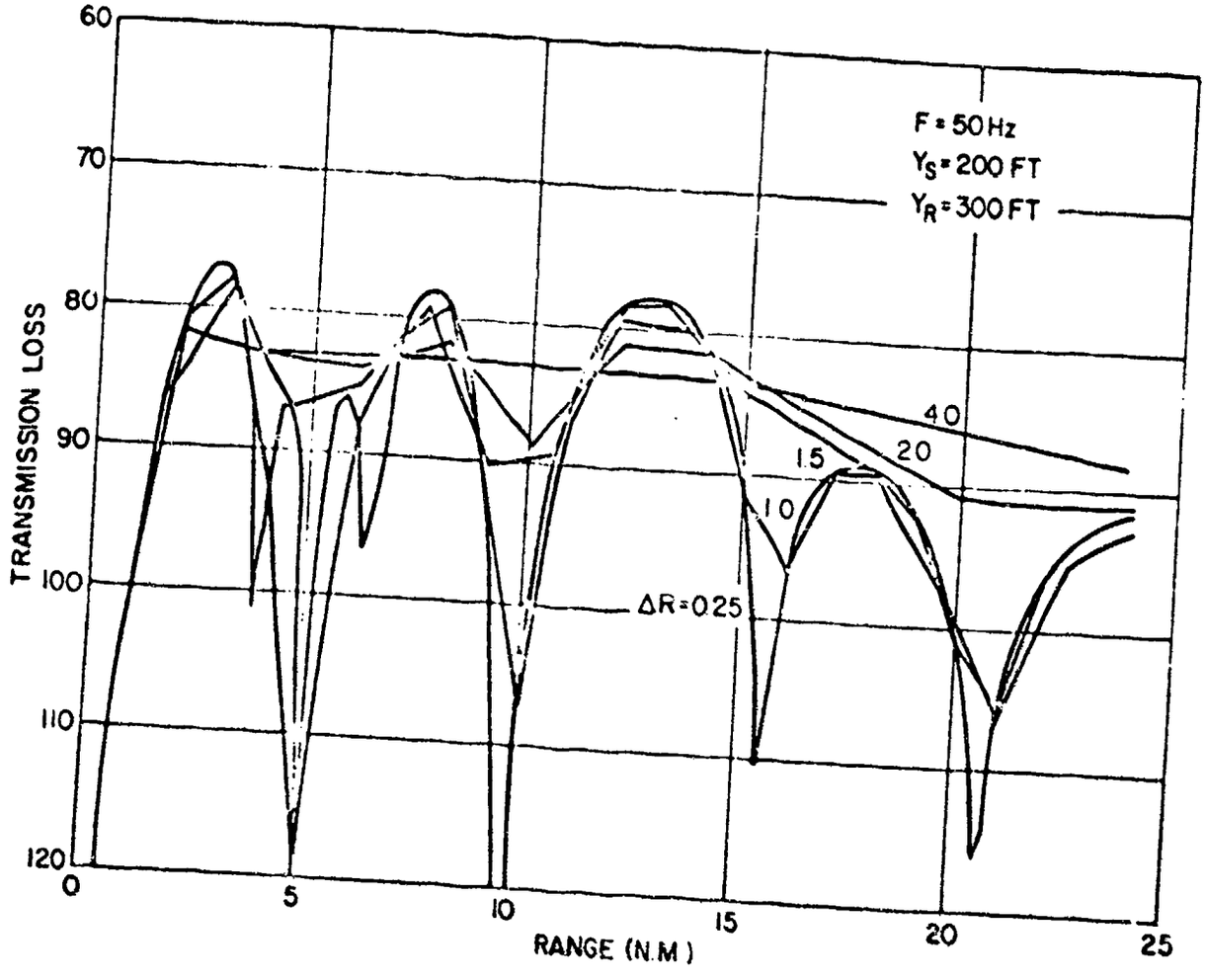

Figure 2-6. "Semi-Coherence" - Automatic Smoothing of Surface-Image Interference with Sampling Interval ΔR (nm)

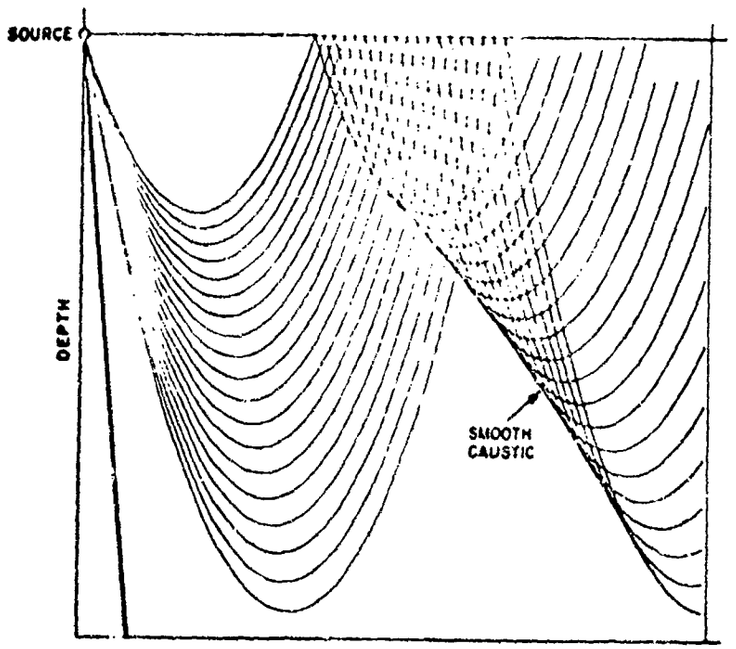

Figure 2-7. Development of a Smooth Caustic in a Pressure-Gradient Profile

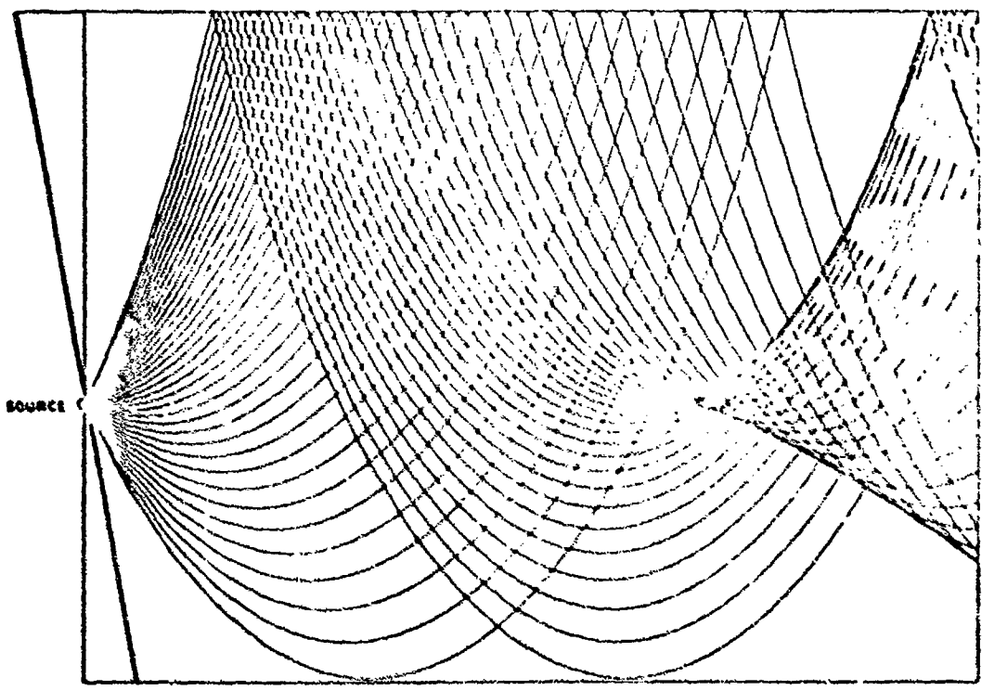

Figure 2-8. Development of a Cusped Caustic in a Pressure-Gradient Profile

Figure 2-9. 25 Hz

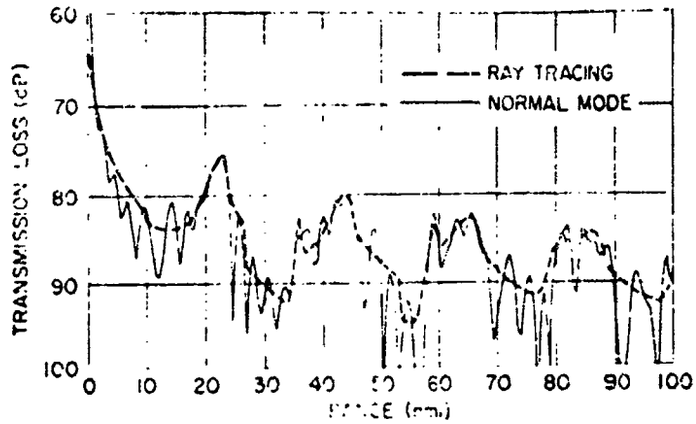

Figure 2-10. 50 Hz

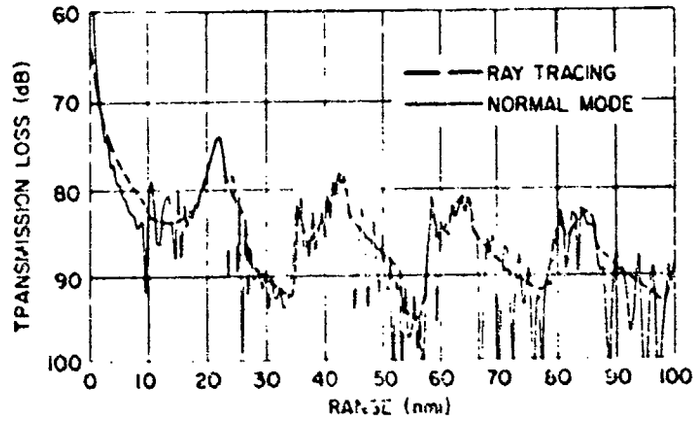

Figure 2-11. 100 Hz

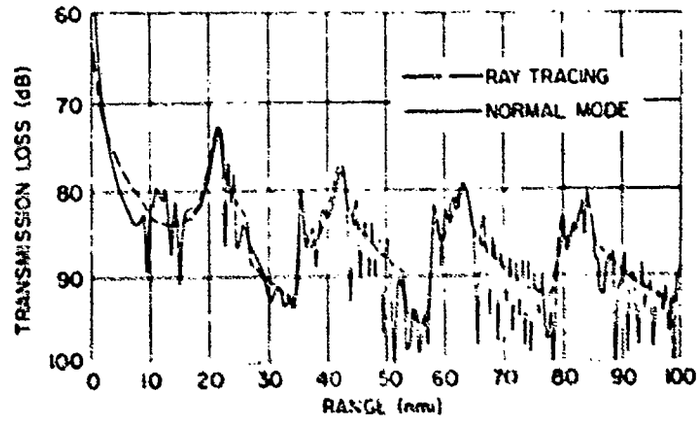

Comparison of FACT ("RAY TRACING") with Normal Modes for Cusped Caustics

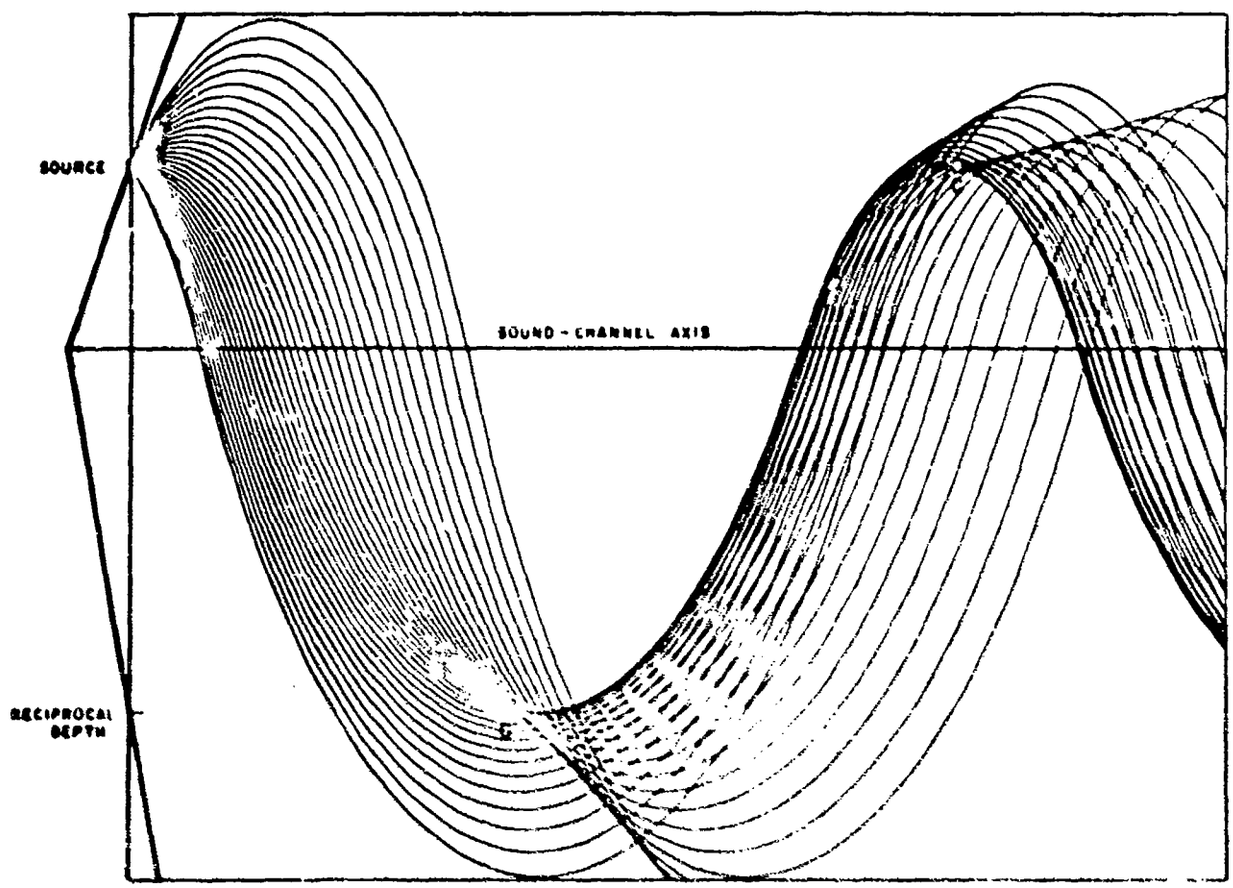

Figure 2-12. Development of a Four-Ray System (Smooth Caustic Near a Cusped Caustic)

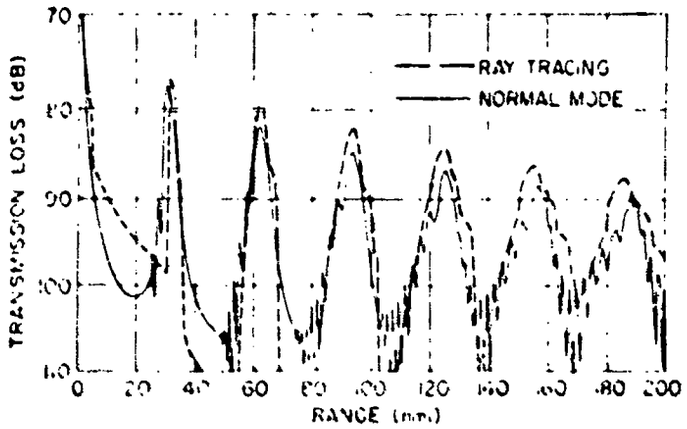

Figure 2-13. 25 Hz

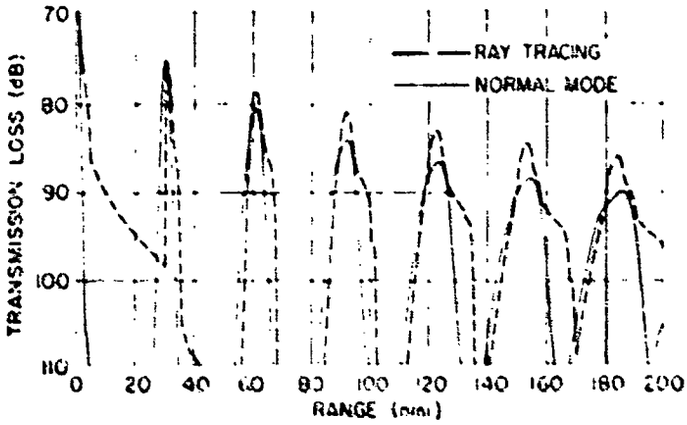

Figure 2-14. 50 Hz

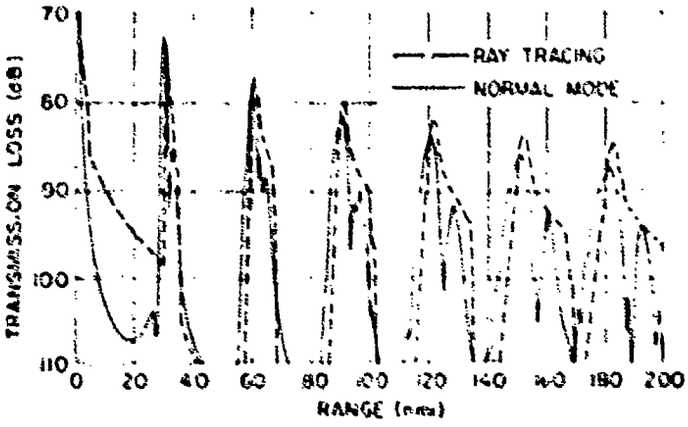

Figure 2-15. 100 Hz

Comparison of FACT ("RAY TRACING") with Normal Modes for Four-Ray Systems

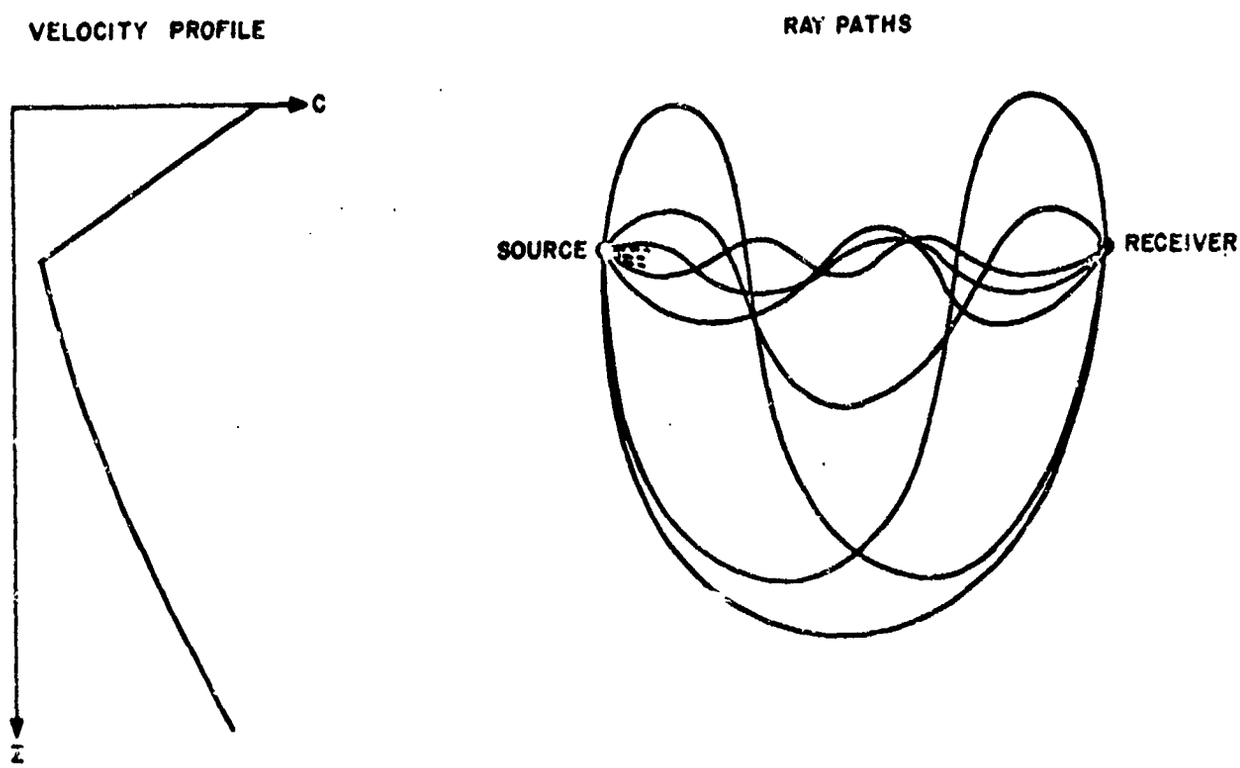

Figure 2-16. Ray Paths between Axial Source and Receiver for a Bilinear Profile

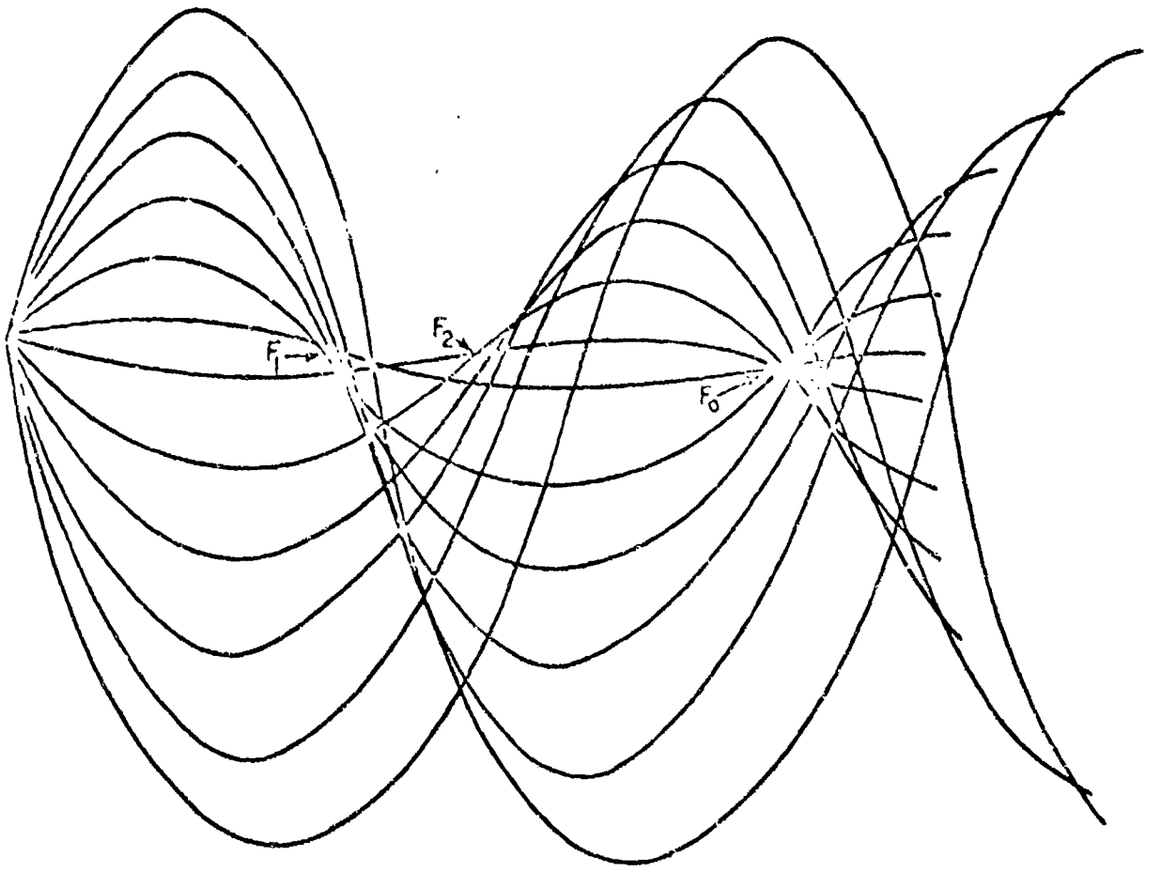

Figure 2-17. Ray Paths from a Source on Axis for an Asymmetric Quadratic Profile

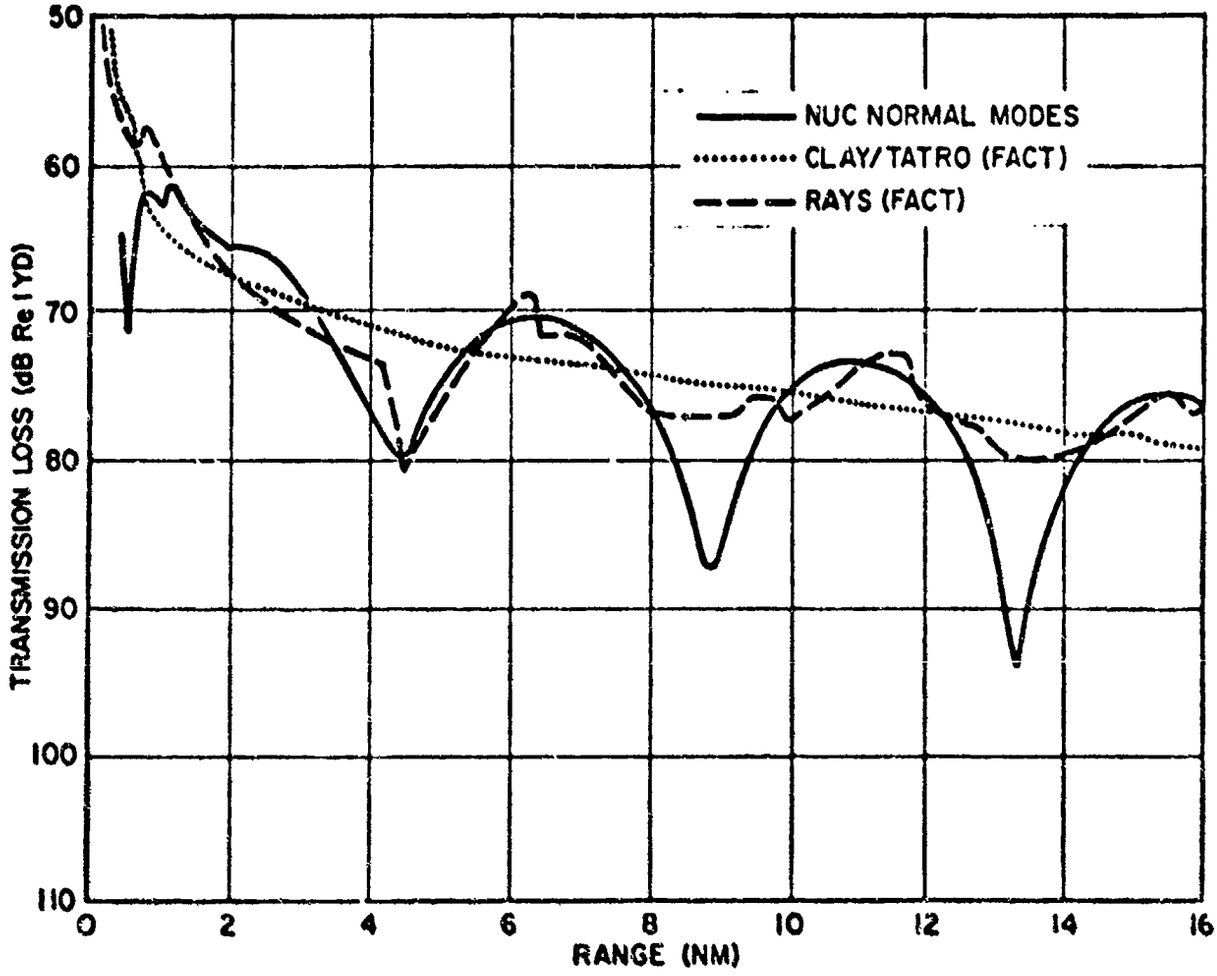

Figure 2-18. Comparison of Surface-Duct Predictions Using Three Models; z_s=300', z_R=90', F=300 Hz

3. MATHEMATICAL DESCRIPTION OF THE FACT MODEL

The previous section contains the background physics and the rationale for the approach employed in FACT. This section documents the mathematical implementation of the approach and Section 4 contains a detailed flow chart of the resulting computer code.

In this section some specific terms are introduced from the jargon of ray tracing. While many of them also appear in the measurement literature, the definitions differ somewhat and are repeated here for conciseness. In ray solutions for transmission loss one attempts to find all significant rays or paths connecting the source and receiver. The precise rays can, in principle, be determined by iterative targeting procedures, however, the excessive running time is unacceptable. More typically a number of rays is traced from the starting point (or receiver) and the ranges at which each ray crosses the source depth are noted. The source-depth crossings of these rays are, in ray jargon, arrivals. If the ray density is adequate, the ray through the desired range is determined by interpolating between arrivals of adjacent rays bracketing the range of interest. Such interpolations are justified when rays are in the same family and of the same arrival order. The arrival order refers to the number of deep cycles the ray has experienced (either refracting at depth or bottom reflecting). Within an arrival order rays are subdivided into classes (RR, RSR, etc.). Within classes additional subdivisions into ray families may be required to assist the interpolation algorithms.

(family 3); and one surface-reflected bottom-reflected or SRBR (family 4). In each family except the last, two or more rays are specified within each layer encompassed by a family. The extreme effects of false caustics are excluded by avoiding rays with horizontal turning points that are just beyond a level where the gradient increases in magnitude. For example, the ray θ_c in Family 1 is traced, but the slightly steeper ray, θ'_c is avoided. The final family (SRBR) includes only the first ray to strike both the surface and the bottom and the steeper of the following two rays:

1. The ray five degrees steeper at the receiver than the first ray;

2. The ray striking the bottom at the effective critical angle of the low-frequency bottom-reflectivity function.

More families may be formed than those described in the example above if the gradient, from one layer to the next, decreases in absolute value as the sound speed increases, thus allowing for maximum-range caustics associated with points of inflection in the velocity profile. In such a case the rays equivalent to θ_c and θ'_c in Figure 3-1 become bounding rays of the new families.

When the rays have been selected, they are traced for half a cycle and three quantities are computed: the range to the first intersection of the source depth for a ray traced upward at angle θ, the range to the second intersection for the same ray, and the period of the ray. From these quantities the ranges to the first and second source-depth intersections for the downgoing ray, as well as the

ranges of all subsequent arrivals, may be computed using the periodicity of the ray in a layered environment.

The range is accumulated as the ray steps through each layer making use of the well-known fact that within each layer the ray trajectory is the arc of a circle. The expression used for the incremental range, ΔR, within a layer between depths y_1 and y_2 (with ray angles θ_1 and θ_2 respectively) is

$$\Delta R = \left| \frac{(y_2 - y_1) \cdot (\cos\theta_2 + \cos\theta_1)}{(\sin\theta_2 + \sin\theta_1)} \right| \qquad (3\text{-}1)$$

This is identical to the more traditional expressions and avoids the numerical problems associated with small gradients. Snell's Law, of course, gives θ_k where

$$\cos\theta_k = \frac{c_k}{c_R} \cos\theta_R \qquad (3\text{-}2)$$

When a ray turns within a layer with gradient g, the range increment to the horizontal turning point is

$$\Delta R = \left| \frac{c_1 \tan\theta_1}{g} \right| \qquad (3\text{-}3)$$

3.2 Smoothing θ-R Curves

After the rays are traced the arrival ranges of all the rays within a family are grouped to form an arrival order. The range to the arrival as a function of the source angle,

θ, is then fit with one of several functions depending upon the family. The purpose of this fitting is to remove false caustics, obtain the relevant parameters of true caustics, and provide continuous analytical functions for $R(\theta)$ which may subsequently be inverted and differentiated to obtain the intensities of all rays through all points of interest.

For all families but the SRBR (and a portion of families containing a cusped caustic) $R(\theta)$ is fitted with one of two types of second order functions:

$$R(\theta) = a + b\left(\theta - \theta_L\right)^{1/2} + c\left(\theta - \theta_L\right) \qquad (3\text{-}4)$$

or families in which the minimum ray, θ_L, just grazes either the surface, the bottom, a local maximum in sound speed, or a decrease in magnitude of the gradient: or

$$R(\theta) = a + b \tan\theta + c \tan^2\theta \qquad (3\text{-}5)$$

if the minimum ray does not meet one of the above criteria.

The first form is chosen for the appropriate families since it permits the presence of one caustic ($R' = 0$) and goes to the proper limiting intensity (0) as $\theta \to \theta_L$ ($R' \to \infty$). This behavior is characteristic of all families except occasionally the first (shallowest). The second form may be required for the first family when the minimal ray just grazes the arrival depth, in which case the intensity is finite for this ray.

The coefficients a, b and c are determined by requiring the function to pass through the two points at the angular

extremes of the family and through one of the following three interior points (in preferential order):

1. The minimum range for the family if less than the range at both endpoints;

2. The maximum range if greater than the range at the endpoints;

3. The second point in the family.

For the last (SRBR) family, $R(\theta)$ is given by

$$R(\theta) = \begin{cases} a + b\left(\theta - \theta_L\right)^{1/2} + c\left(\theta - \theta_L\right) \\ \text{or} \\ \dfrac{1}{d \tan \theta + e} \end{cases} . \qquad (3\text{-}6)$$

The first expression is used for angles less than the critical ray on the bottom, and the second is used for steeper rays. The coefficients a through e are determined by requiring $R(\theta)$ to pass through the ranges of the two traced rays, continuity of $R'(\theta)$ (and hence intensity) at the critical ray, and the proper limiting form (isovelocity medium) for $R'(\theta)$ as $\theta \rightarrow 90$ degrees. (Arrivals of rays striking the bottom at more than the critical ray are ignored after the fourth bottom bounce.) A subsequent section is devoted exclusively to the treatment of cusped caustics since it depends upon much of the next section.

3.3 Computing Ray Intensities

The intensity of an arrival is given by:

$$I = \frac{\cos \theta}{R \sin \theta' \left(\frac{\partial R}{\partial \theta}\right)_{y'}} , \qquad (3\text{-}7)$$

where $\theta(R)$ is given by the above functional forms, $\theta'(R)$ (the angle of the ray at the receiver) by Snell's Law, and $(\partial R/\partial \theta)_y$, by differentiating the functions for $R(\theta)$. Modifying this intensity are volume-absorption and bottom-reflection losses where appropriate. The θ-R curves for the typical arrival order in the example of Figure 3-1 are shown in Figure 3-2. The corresponding fitted curves used in the program would differ only for the first family (Figure 3-3a). In this instance the rigorous ray result (solid curve) contains a true caustic, C, and a false caustic, C', whereas the fitted curve (dashed) contains only one caustic. The corresponding I-R and total I-R curves (Figures 3-3b and 3-3c) indicate a significant change in intensities when the false caustic is removed.

The asymptotic intensity at a smooth caustic is given by

$$I_c = \frac{2^{5/3}\, \pi A i^2(0)\ \ \sin^{1/3}\theta \cos\theta}{c^{1/3}} \left(\frac{\omega}{R \sin\theta' \left(\frac{\partial^2 R}{\partial \theta^2}\right)_{y'}}\right)^{2/3} \omega^{1/3} \qquad (3\text{-}8)$$

where $Ai(0)$ is the Airy function evaluated at zero, c is the sound speed at the source, and ω is the angular frequency. The field in the vicinity of the caustic is then

$$I(R) = I_C \cdot \frac{R_C}{R} \quad \frac{Ai^2(-x)}{Ai^2(0)} \qquad (3\text{-}9)$$

where

$$x = \pm\left|\alpha(R-R_C)\right| \qquad (3\text{-}10)$$

and

$$\alpha = \frac{2^{1/3} \sin^{2/3}\theta}{\left(\frac{\partial^2 R}{\partial \theta^2}\right)_y^{1/3}} \left(\frac{\omega}{c}\right)^{2/3} \qquad (3\text{-}11)$$

The sign of x is chosen as positive for points in the illuminated region and negative for those in the shadow-zone. The field in the illuminated region is rapidly oscillatory because of the two-ray interference (solid curve in Figure 3-4). The full description of the field is used near the caustic, while in the oscillatory region the intensity is given by the rms summation of the two paths using their actual computed intensities (dashed curve in Figure 3-4). The transition point corresponds to the first point (x = 1.77) of 90-degree phase difference (allowing for the -90 degree phase shift of the one ray which has touched the caustic). In practice the caustic field is extended into the shadow zone until it is 40 dB below the caustic value (x = -3.5). The shadow-zone field is considered to be propagating at the angle of the caustic ray at the source depth (and to have an angle at the receiver corresponding to the same ray).

3.4 Treatment of Cusped Caustics

For cases where the source and receiver are at the same depth a cusped caustic forms on the zero-degree ray at

each return to the receiver depth. Two types of (smoothed) θ-R curves are possible corresponding to simple three-ray systems (Figures 3-5a) or four-ray systems (Figure 3-5b). In the latter case the rays corresponding to those in the one-ray region of Figure 3-5a, form a smooth caustic of their own at (R_c', θ_c').

In both cases the three-ray region is treated by fitting the branch with a smooth extremal (connecting points a and b)

$$R(\theta) = R_c + \frac{\theta^2}{\beta} \qquad (3\text{-}12)$$

and the branch joining the cusp with finite slope by

$$R(\theta) = R_c + \frac{\theta}{\gamma} \qquad (3\text{-}13)$$

β and γ are determined by the extremals of the family. For the case of Figure 3-5a a similar fit is obtained for the one-ray region using a possibly different value of γ.

The nonuniform approximation used for calculating the intensity of the field near the cusped caustic is given by

$$I = \frac{1}{\pi}\left(\frac{2\pi\beta}{\lambda}\right)^{1/2}\left(\frac{\cos\theta}{R}\right)\left|\overline{Pe(0,Y)}\right|^2 , \qquad (3\text{-}14)$$

where λ is the wavelength, θ is the ray angle at the source or receiver (which are at the same depth), β is the "cusp parameter", and $\overline{Pe(0,Y)}$ is the rms average of the Pearcey function Pe(X,Y) along its axis (X=0). The argument Y is

Between $Y = \sqrt{4\pi}$ and $Y = 2$, the square of the modulus of $Pe(0,Y)$ is used in tabular form. The resultant curve for $[\overline{Pe(0,Y)}]^2$ is plotted in Figure 3-6b.

In the case of a four-ray system, the field associated with the two intersecting branches of the θ-R curve for points interior to the cusp is computed as above. For the branch forming the smooth caustic at θ_c' (Figure 3-5b), the smooth-caustic parameters are computed and the field associated with each portion of this branch is estimated. For the portion of the branch corresponding to rays steeper than the smooth-caustic ray ($\theta > \theta_c'$), and in the shadow zone ($R < R_c'$), the smooth-caustic fields are used. For the portion of the branch between $\theta = \theta_c'$ and $\theta = 0$, the maximum of either the smooth-caustic field or the cusped-caustic field (as given by Equation 3-14) is used. The result is a continuous transition from the peak field associated with the cusp to the rapidly attenuated field associated with the shadow-zone of the smooth caustic.

For severe cases where the smooth and cusped caustics are separated by fractions of a wavelength a more accurate evaluation of the field requires that the smooth- and cusped-caustic fields be added on a phase basis rather than on the rms basis used here. Such an approach is currently beyond the scope of FACT and in such instances one might expect fields slightly stronger (as much as 3 dB) than predicted.

While this completes the computation of the field, the arrival-structure option requires the angle and intensity of each path from a given range. In the three-ray region,

it is assumed that each of the three paths has the same intensity and that the angles are obtained from Equations 3-12 and 3-13. For a simple cusped caustic the single ray carries all the energy. For four-ray systems the angles for the branch outside the cusp are computed as for any smooth caustic with the corresponding partitioning of energy.

3.5 Coherent Summation of Paths

There are two situations in which low-frequency coherence effects are expected (Figure 3-7). In the first situation (only one depth of interest is shallow), the total intensity, I_2, is given by the phased sum of the intensities of the two rays shown, and may be approximated by

$$I_2 = 4I_1 \sin^2\left(\frac{\omega D \sin\theta}{c}\right), \qquad (3\text{-}19)$$

where I_1 is the single-path intensity (assumed equal for both paths), and D the depth of interest.

When both depths of interest are shallow (Figure 3-7b), four paths must be phase-summed and

$$I_4 = 16I_1 \sin^2\left(\frac{\omega D_1 \sin\theta}{c}\right)\sin^2\left(\frac{\omega D_2 \sin\theta}{c}\right). \qquad (3\text{-}20)$$

For large D and/or ω the variation in angle, θ, with range may produce oscillations which are inadequately sampled by the specified range step. Rewriting the two-path sum as

$$I_2 = 2I_1\left(1 - \delta\cos\left(\frac{2\omega D \sin\theta}{c}\right)\right) \qquad (3\text{-}21)$$

we see that δ=1 yields the previous expression whereas δ=0 yields the standard incoherent sum. δ then plays the role of a coherence factor, and without inferring any physical significance, it may be used to provide a smooth transition from a fully coherent to incoherent sum as the sampling interval becomes inadequate. For a given family the number of cycles of the interference pattern of frequency f is given by

$$N_c = \frac{2Df}{c} (\sin\theta_{max} - \sin\theta_{min}) \qquad (3\text{-}21)$$

where θ_{max} and θ_{min} are the bounding rays of the family. The number of range points (at interval δR) sampled per cycle of interference for a given arrival order of total range-span ΔR is then

$$N_p = \frac{\Delta R}{N_c \delta R} \qquad (3\text{-}22)$$

The smoothing, or coherence, factor δ is then determined by

$$\delta = \begin{cases} 0 & N_p \leq 8/3 \\ \dfrac{N_p - 8/3}{6 - 8/3} & 8/3 < N_p < 6 \\ 1 & 6 \leq N_p \end{cases} \qquad (3\text{-}23)$$

The net effect when applied to the 2 or 4-path cases is a smooth transition from fully coherent to incoherent summation as, for example, the sampling interval or the frequency increases.

It should be noted that the accuracy of the basic approximation is degraded as the ray angle becomes very shallow or the source (receiver) becomes very deep. In such cases the approximation for the phase difference becomes poorer as does the assumption of equal ray amplitudes. Also since the calculation takes two or four families in an arrival order and replaces them with one modified family the range extent of the order is reduced somewhat. To prevent significant errors this approximation is permitted only if the up- and down-going arrivals at the source (receiver) of the shallowest ray in the family are separated by no more than 2 nautical miles.

3.6 Low-Frequency Cut-Off Effects

The ray equivalent of the first propagating mode satisfies the phase-integral relationship

$$\oint k_z dz = \Delta\phi \qquad (3\text{-}24)$$

where the integral is taken over a full ray cycle,

$$k_z = \frac{2\pi}{\lambda} \sin\theta(z) \qquad (3\text{-}25)$$

and $\Delta\phi$ corresponds to the discrete phase shifts accumulated by the ray over a cycle (π for surface reflections plus $\pi/2$ for each horizontal reversal). At the relevant sound-channel axis (which will be the surface for half-channel propagation) this ray has angle θ_o. The intensities of all rays shallower than θ_o are reduced by the factor $\sin^2\theta_x/\sin^2\theta_o$ where θ_x is the ray angle at the axis.

3.7 Axis-to-Axis Propagation

The "period" of the axial ray in a sound-speed profile with a discontinuous second derivative at the smooth axis (i.e. the distance to F_o in Figure 2-17) is given by

$$P_o = \pi \left(\left(\frac{c_o}{c''_-} \right)^{1/2} + \left(\frac{c_o}{c''_+} \right)^{1/2} \right) \qquad (3\text{-}26)$$

where c_o is the axial sound speed, and c''_- and c''_+ are the values of the second derivative of $c(z)$ just above and just below the axis.

These derivatives are estimated by the following procedure (illustrated in Figure 3-8):

1. Determine whether or not the source and receiver are contained in the two layers defining the axis (z_x), and if they are, in the smaller region defined by z_- and z_+.

2. If z_S and $z_R \notin (z_-, z_+)$ exit without applying axis corrections. Otherwise compute c''_- and c''_+ from

$$c''_* = \frac{2(c(z_*) - c(z_x))}{(z_* - z_x)^2} \qquad *=-,+ \qquad (3\text{-}27)$$

i.e. fit $c(z)$ with two parabolas, one through z_- and z_x, the other through z_+ and z_x, both with their minima at z_x.

3. Determine the ray which when traced in the segmented profile has period P_o, from

$$\tan\theta_x = \frac{P_o}{2\left(\frac{1}{g_+} - \frac{1}{g_-}\right) c_x} \qquad (3\text{-}28)$$

where q_- and q_+ are the gradients above and below the axis respectively.

4. If z_S and z_R are both between the turning points of this ray, move both z_S and z_R to the nearer of the two turning points.

In this procedure the important characteristics of the axis are governed by the two closest layers: and the user should bear this in mind when selecting points for the input profile.*

3.8 Surface-Ducted Propagation

The transmission loss as a function of range R (in nm) in the surface duct (excluding volumetric absorption) is given by

$$TL(R) = 22 + 10\text{Log}_{10}\ (R \cdot \Delta\theta) + b \cdot R \qquad (3\text{-}29)$$

where $\Delta\theta$ is the angle at the surface of the ray just grazing the bottom of the duct and b contains the duct-leakage and rough-surface losses

$$b = 14.88\times10^{-5}\ f_k^{-5/3}\ g_z^{-1/3}\ z_D^{-3} + W\ f_k^{1/2}\ z_D^{-1/2} \qquad (3\text{-}30)$$

In the above expression f_k is the frequency in kilohertz, g_z the magnitude of the below-duct gradient, z_D the duct depth (in ft), and W the wave-height factor which is sea-state (SS) dependent:

---

* This approach to axis-to-axis propagation differs somewhat from that originally incorporated in FACT thanks to several helpful comments from Mr. C. L. Bartberger.

$$W = \begin{cases} 9 & SS < 3 \\ 13.5 & SS = 3 \\ 18 & SS > 3 \end{cases} \qquad (3\text{-}31)$$

3.9 Shallow-Water Module

The special-purpose shallow-water module computes the loss for cases where ray computations would be too lengthy because of the combination of very shallow water and a bottom which is perfectly reflecting below critical angle. The approximation assumes a homogeneous medium and replaces the summation of all paths by an approximate integral. Surface-image interference effects are included where their range-averaged effect leads to a result appreciably different from the incoherent combination of paths. The bottom is treated as having an intensity reflection coefficient of unity up to the critical angle, θ_c, and a uniform loss given by the loss at normal incidence, L_{90}, at steeper angles. The contributions of rays steeper than θ_c are included for only one bottom-reflected order since for higher orders they are always negligible compared to the other available paths. The intensity at any range then consists of the contributions of the direct and bottom-reflected paths.

$$I = I_D + I_{BB} \qquad (3\text{-}32)$$

The direct-path contribution is computed by summing incoherently the direct and surface reflected paths out to the range, R_{rms}, where the phase difference between the two paths is $-\pi/2$, and summing coherently beyond:

$$I = \begin{cases} 2/R^2 & \text{for } R \leq R_{rms} \\ \frac{4}{R^2} \sin^2\left(\frac{\Delta\phi}{2}\right) & \text{for } R > R_{rms} \end{cases} \qquad (3\text{-}33)$$

where

$$\Delta\phi = \frac{4\pi D_1 D_2}{\lambda R} \qquad (3\text{-}34)$$

and $\Delta\phi = \pi/2$ at R_{rms}:

$$R_{rms} = \frac{8 D_1 D_2}{\lambda} \qquad (3\text{-}35)$$

For bottom-bounce paths the range is divided into two regions $R < R_{BB}$ and $R \geq R_{BB}$ where

$$R_{BB} = 2z_B/\theta_c \qquad (3\text{-}36)$$

is approximately the period of the critical ray in a homogeneous region of depth z_B. For $R < R_{BB}$

$$I = \frac{1}{R^2 + (2z_B)^2} \cdot L_{90} \cdot F' \qquad (3\text{-}37)$$

where F' contains the surface-image interference effects averaged over all rays between θ_c and $\pi/2$:

$$F' = \frac{16}{\pi/2 - \theta_c} \int_{\theta_c}^{\pi/2} \sin^2\left(\frac{\omega D_1 \sin\theta}{c}\right) \sin^2\left(\frac{\omega D_2 \sin\theta}{c}\right) d\theta$$

$$= \frac{16}{\pi/2 - \theta_c} \cdot [G(u_1, u_2, \pi/2) - G(u_1, u_2, \theta_c)] \qquad (3\text{-}38)$$

where $u_k = \omega D_k \sin\theta / c$ for $k = 1, 2$ and

$$G(u_1,u_2,\theta) = \frac{\theta}{4}\left\{1 - \frac{\sin u_1}{u_1} - \frac{\sin u_2}{u_2}\right.$$

$$\left. + \frac{\sin(u_1-u_2)}{2(u_1-u_2)} + \frac{\sin(u_1+u_2)}{2(u_1+u_2)}\right\} \quad u_1 \neq u_2, \tag{3-39}$$

$$= \frac{\theta}{4}\left\{\frac{3}{2} - \frac{2\sin u_1}{u_1} + \frac{\sin 2u_1}{4u_1}\right\}, \quad u_2 = u_1 \tag{3-40}$$

For $R \geq R_{BB}$

$$I_{BB} = \sum_{i=1}^{N} I_i F_i \tag{3-41}$$

where F_i contains the surface-image interference effects on the i-th path, N is the maximum number of bottom bounces at range R of rays shallower than θ_c, and

$$I_i = \frac{1}{R^2 + (2iz_B)^2} \tag{3-42}$$

Replacing the summation by an integral over i, and noting that for each range and value of i a ray of angle θ may be identified:

$$\tan\theta = \frac{2z_B\, i}{R} \tag{3-43}$$

we obtain

$$I_{BB} \simeq \frac{8}{Rz_B} \int_0^{\theta_c} \sin^2\left(\frac{\omega D_1 \sin\theta}{c}\right) \sin^2\left(\frac{\omega D_2 \sin\theta}{c}\right) d\theta$$

$$\simeq \frac{8}{Rz_B} G(u_1, u_2, \theta_c) \qquad (3\text{-}44)$$

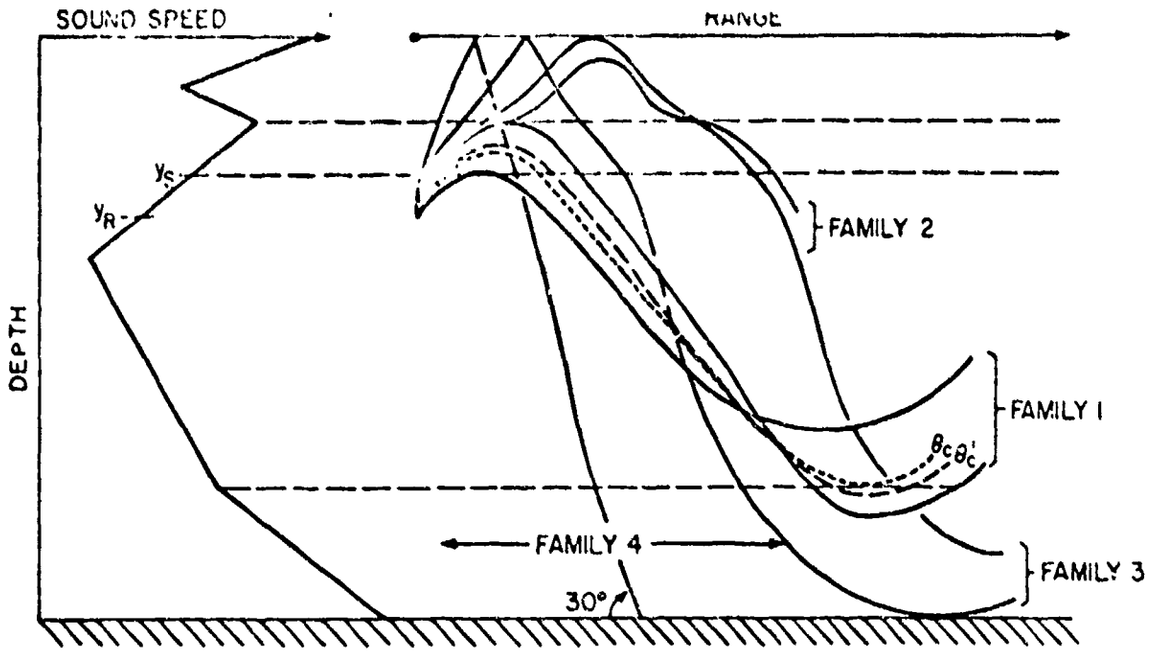

Figure 3-1. Typical Ray Families in FACT

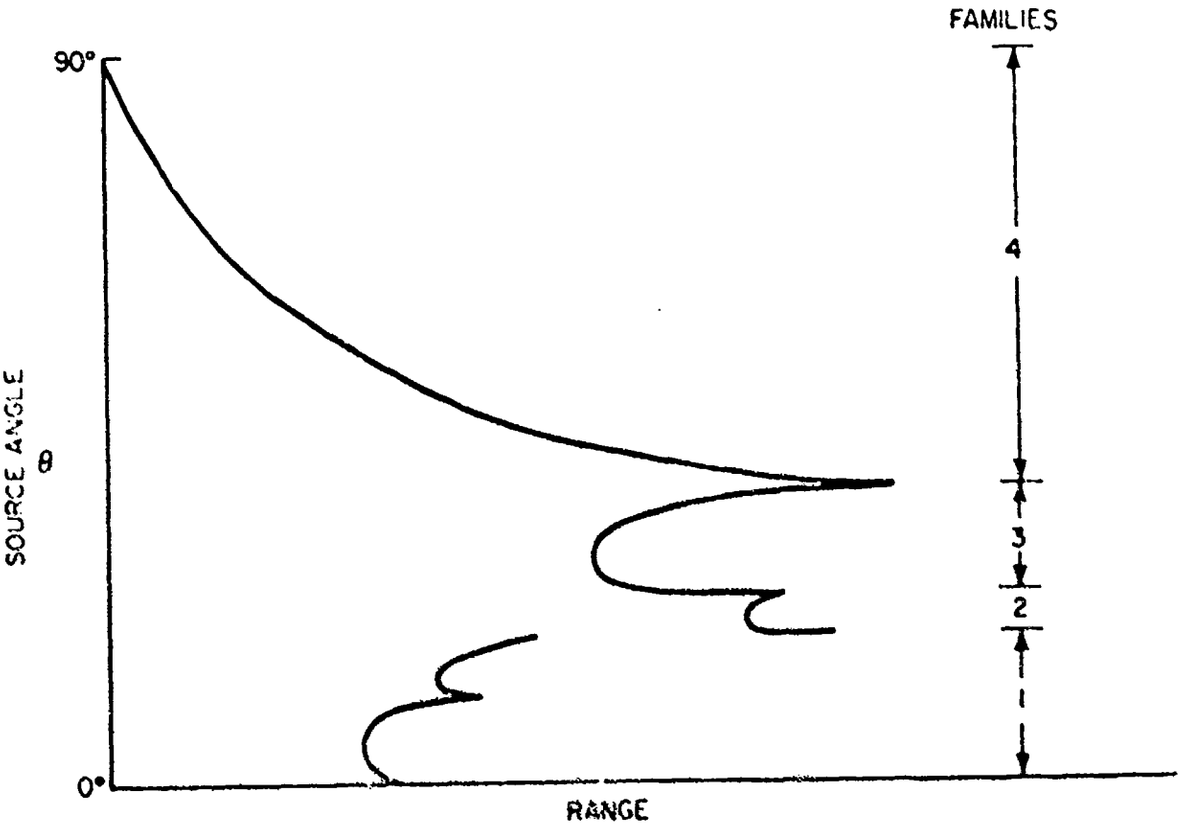

Figure 3-2. θ-R Curves for Typical Arrival Order of Ray Families in Figure 3-1

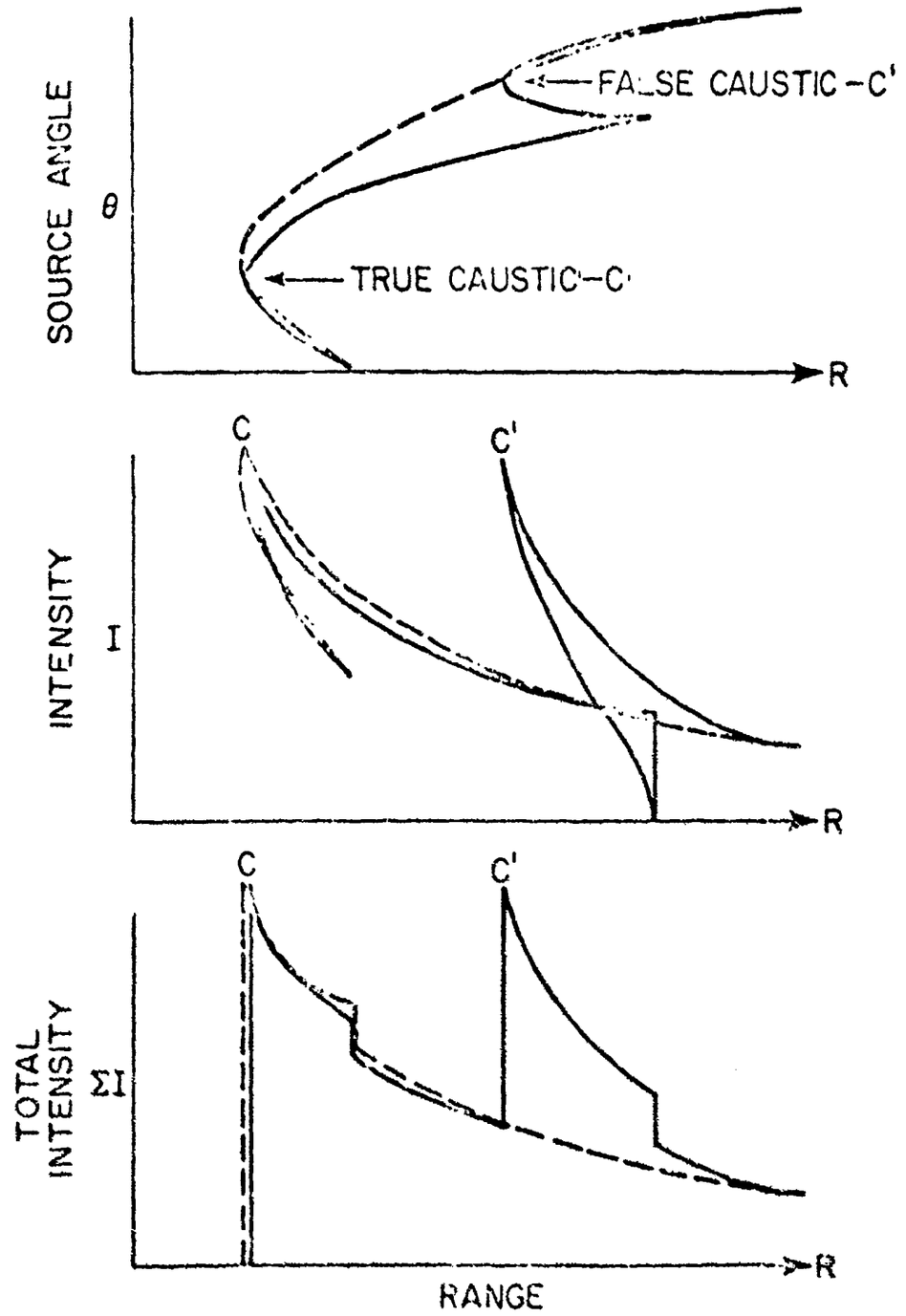

Figure 3-3. Comparison of Traced (___) and Fitted (---) Angle and Intensity vs Range Curves for Family 1 of Figure 3-2

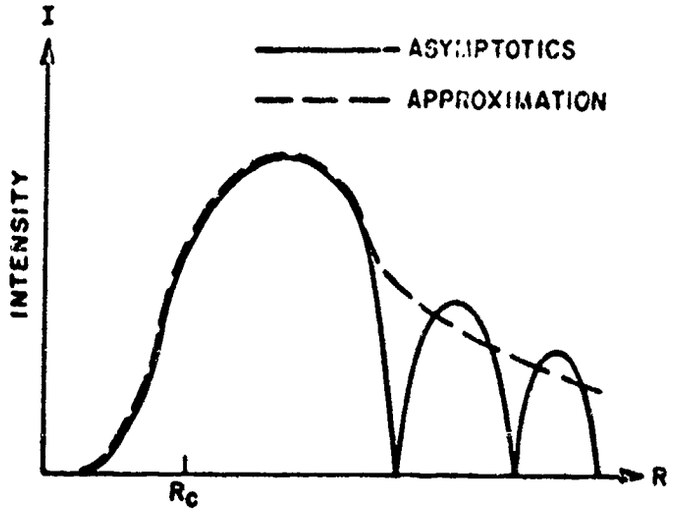

Figure 3-4. Comparison of Full-Asymptotic and FACT Approximation Treatments of Intensity Near a Smooth Caustic

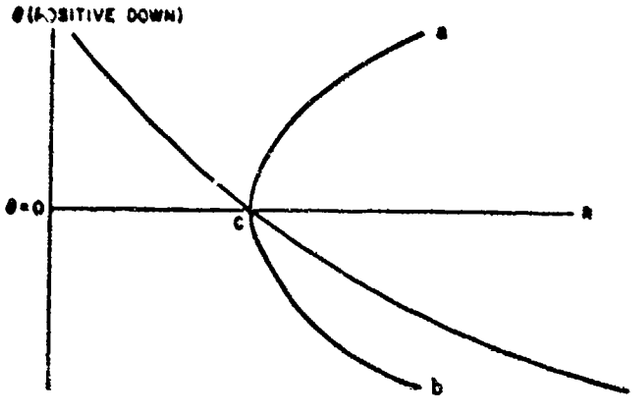

Figure 3-5a. Three-Ray System of Figure 2-8

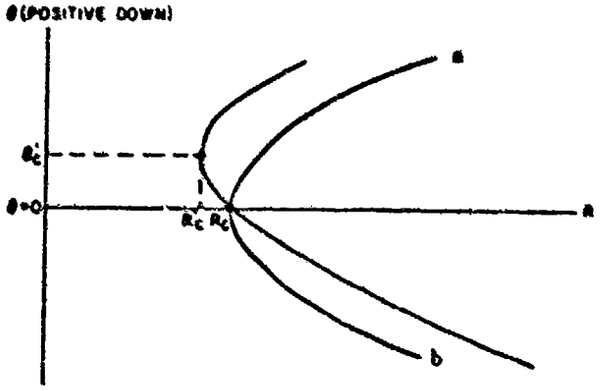

Figure 3-5b. Four-Ray System of Figure 2-12

θ-R Curves for Cusped Caustics

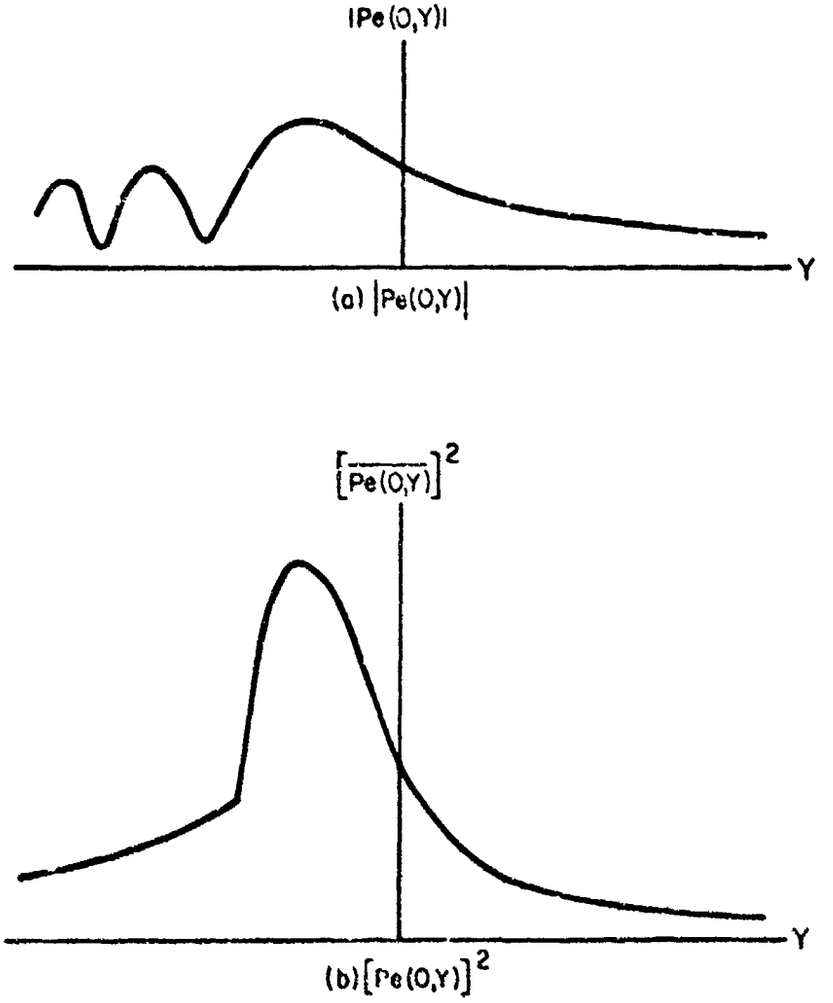

Figure 3-6. Comparison of Full-Asymptotic and FACT-Approximation Treatments of Intensity Near a Cusped Caustic

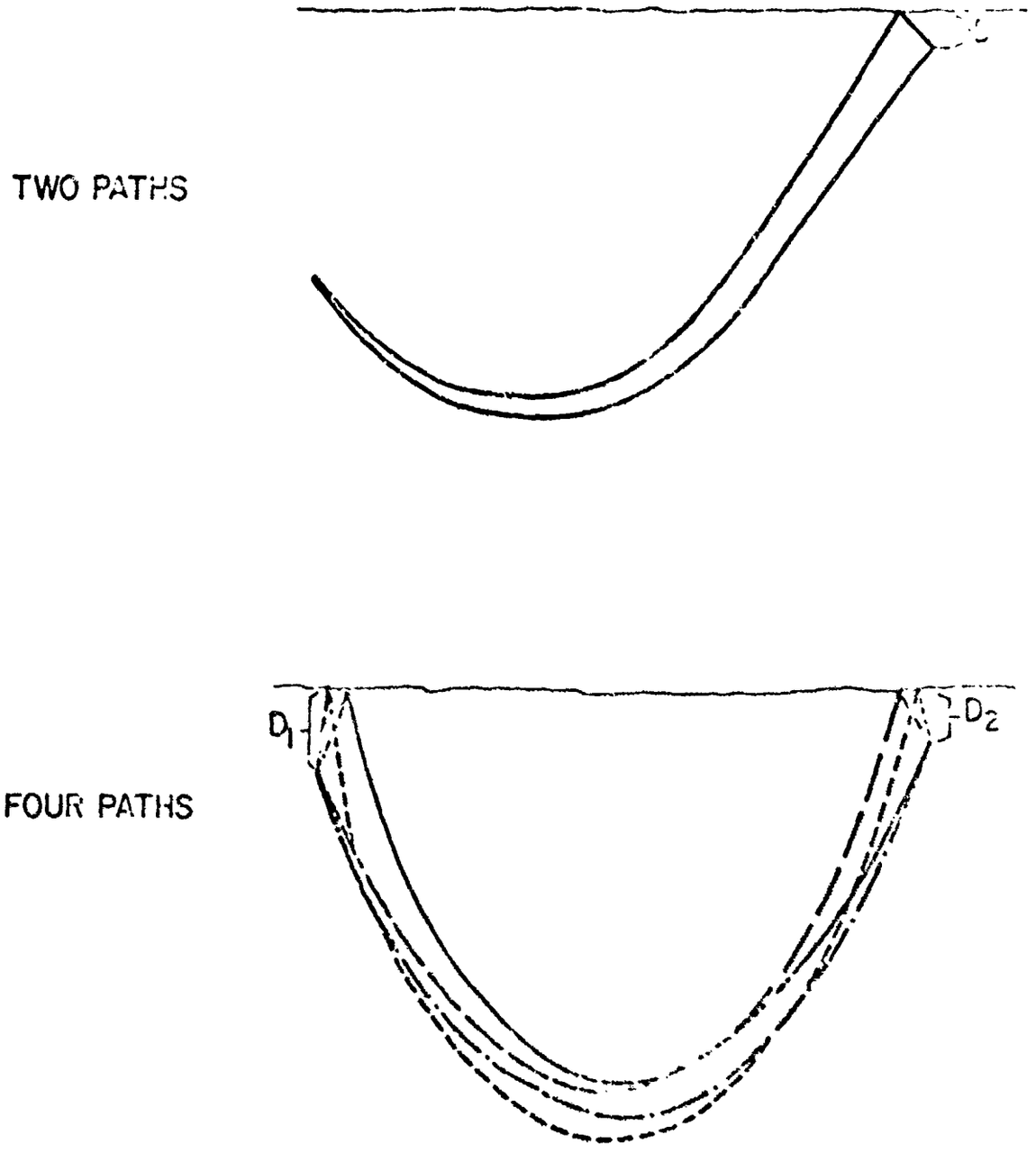

Figure 3-7. Conditions Requiring Coherent Addition at Low Frequencies

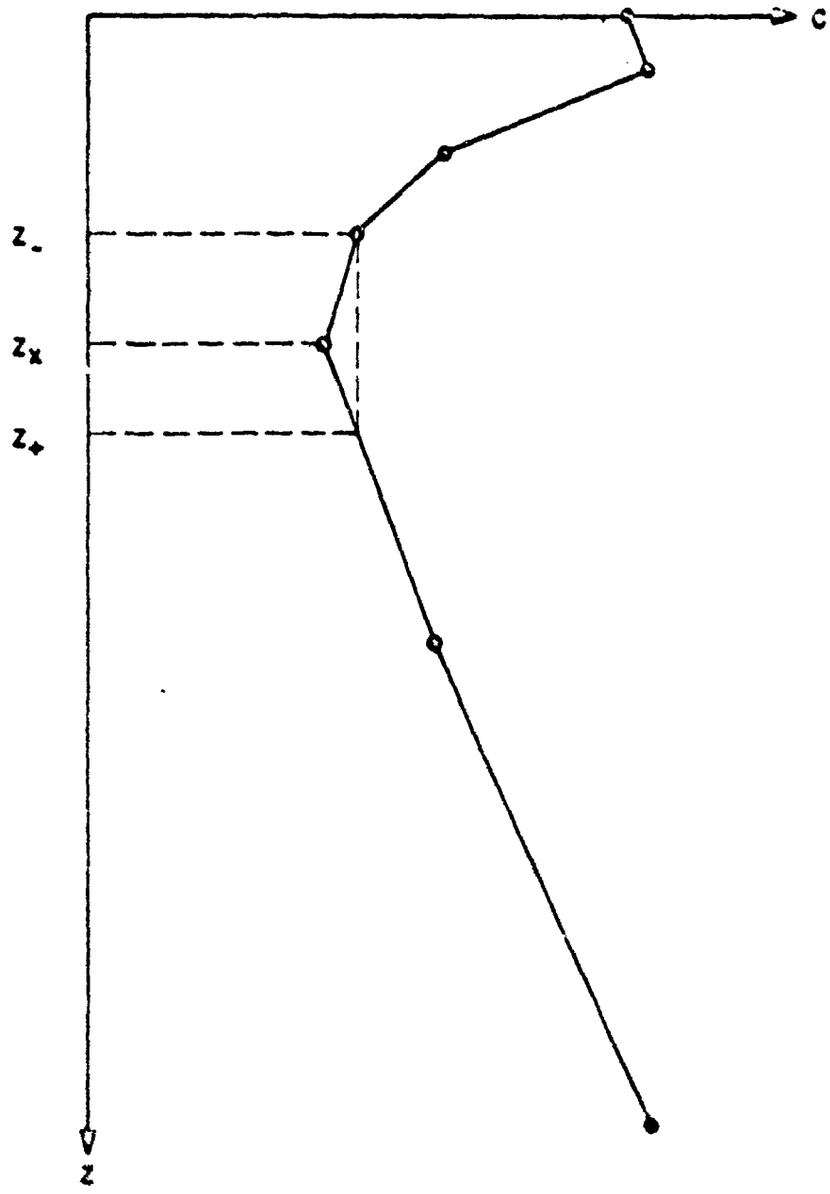

Figure 3-8. Definition of Axial Region for Fitting with Smooth Profile

REFERENCES

C. L. Baker, FACT Transmission Loss Model Development for Acoustic Environmental Support Detachment - Final Report, Ocean Data Systems, Inc., June 30, 1973, on Contract N00014-73-C-0131.

C. G. Bassett and P. M. Wolff, Fleet Numerical Weather Central Bottom Loss Values (U), FNWC, PRT#2, August 1970. (CONFIDENTIAL)

L. M. Brekhovskikh, Waves in Layered Media, Academic Press, New York, 1960a, p 484.

_____, 1960b, pp 452-3.

H. P. Bucker, "Sound Propagation in a Channel with Lossy Boundaries", J. Acoustic. Soc. Am., Vol 48 (1970), pp 1187-1194.

R. E. Christensen, J. Frank and O. Kaufman, Proposed Navy Interim Standard Bottom Loss Curves at Frequencies From 1.0 to 3.5 kHz (U), NOO TN 9320-02-72, 7 September 1972. (CONFIDENTIAL)

C. S. Clay, "Sound Transmission in a Half Channel and Surface Duct", Technical Notes on Sound Propagation in the Sea, Vol 2, Meteorology International, Inc., Monterey. California, 1968.

J. Cummins, Ed., Preliminary Data Report for Surface Duct Sonar Measurements, Cruise II (SUDS 1 1972), NUC TN 883, November 1972.

F. E. DeAngelis and C. W. Spofford, Surface-Image Interference Effects in Long-Range Active Sonar Systems (U), 20 February 1970, Bell Laboratories on Contract N00014-69-C-0074. (SECRET)

J. S. Hanna, "Interference and the Frequency Dependence of Transmission Loss" (Reference 20), Project Jezebel 20th Systems Study Report (U), Vol 2, 1 November 1970, Bell Laboratories on Contracts N00039-69-C-3523 and N00039-71-C-0307. (SECRET)

R. L. Holford and C. W. Spofford, Long Range Acoustic Propagation Program Final Report (U), April 1973, Bell Laboratories on Contract N00014-69-C-0088 (CONFIDENTIAL), Reference 5.

R. L. Holford, Continuation of LRAPP (U), February 1972, Bell Laboratories on Contract N00014-69-C-0088 (CONFIDENTIAL), Reference 8, "Modification to Ray Theory Near Cusped Caustics". (UNCLASSIFIED)

F. M. Labianca, Continuation of LRAPP (U) 1972, (CONFIDENTIAL), Reference 8, "Critique of C. S. Clay's 'Sound Transmission in a Half Channel and Surface Duct'". (UNCLASSIFIED)

D. Ludwig, "Uniform Asymptotic Expansions at a Caustic", Commun. Pure Appl. Math., Vol 19 (1966), pp 215-250.

H. W. March and M. Schulkin, Report on the Status of Project AMOS, U. S. Naval Underwater Sound Laboratory, New London, Conn., 9 May 1967.

H. E. Morris, Comparison of Propagation Prediction Models with SUDS I Acoustic Data, NUC-TP-377, April 1974.

Parka I Report, Maury Center Report 003, 1969, p 65. (SECRET)

M. A. Pedersen, "Acoustic Intensity Anomalies Introduced by Constant Velocity Gradients", J. Acoustic. Soc. Am., Vol 33 (1961), pp 465-474.

D. A. Sachs and A. Silbiger, "Focusing and Refraction of Harmonic Sound and Transient Pulses in Stratified Media", J. Acoust. Soc. Am., Vol 49 (1971), pp 824-840.

C. W. Spofford, Continuation of LRAPP (U), 1972a, (CONFIDENTIAL), Reference 5, "An Ultra-Fast Special-Purpose Ray-Tracing Program". (UNCLASSIFIED)

C. W. Spofford, Continuation of LRAPP (U), 1972b, (CONFIDENTIAL), Reference 6, "Ray-Tracing Program for Modeling Arrival Structure and Noise Directivity". (UNCLASSIFIED)

C. W. Spofford, Frequency-Dependent Ray Selection for Half-Channel and Axis-to-Axis Transmission, Internal Bell Laboratories MM72-6213-6, January 21, 1972c.

C. W. Spofford, Long Range Acoustic Propagation Program Final Report (U), 1973a, (CONFIDENTIAL, Reference 4, "Implementation of Cusped Caustics in the Fast Program". (UNCLASSIFIED)

C. W. Spofford, A Synopsis of the AESD Workshop on Acoustic-Propagation Modeling by Non-Ray Tracing Techniques, 22-25 May 1973, Washington, D. C.", AESD TN-73-05, November 1973b.

W. H. Thorp, "Deep Ocean Sound Attenuation in the Sub- and Low-kilocycle-per-second Region", J. Acoust. Soc. Am., Vol 38 (1965), p 648.

A. G. D. Watson, The Effect of the Earth's Sphericity in Temperature, Pressure and Salinity, Adm. Res. Lab/ Rpt. ARL/N29/L (1958).

DISTRIBUTION LIST

AAI Corporation

Advanced Research Projects Agency - 2 Copies

Air Antisubmarine Squadron 21, 22, 24, 28, 29, 30, 31, 32, 33, 37, 38, 41, 71, 72, 73, 81, 82 and 83

Air Antisubmarine Wing One

Air Test and Evaluation Squadron 1, 4 and 5

Air Test and Evaluation Squadron 5 - Detachment Oceana

Andrulis Research Corp.

Antarctic Development Squadron 6

Antisubmarine Warfare Force - Detachment Rota, Sigonella

Antisubmarine Warfare Systems Project

Antisubmarine Warfare Wing Pacific

Applied Research Lab. Pa. State U.

Applied Research Lab. U. of Texas

Arthur D. Little, Inc.

Assistant Secretary of the Navy for Research and Development

Atlantic Fleet ASW Tactical School

Bell Telephone Laboratory

B-K Dynamics, Inc.

Bolt, Beranek and Newman, Inc.

Bunker-Ramo Corporation

Carrier Antisubmarine Air Group Reserve 70, 80

Central Intelligence Agency

Chesapeake Instruments Corporation

Chief of Naval Material

Chief of Naval Operations

Commander Seventh Fleet

Commander Sixth Fleet

Commander Third Fleet

Commander-in-Chief Atlantic

Commander-in-Chief Atlantic Fleet

Commander-in-Chief U.S. Naval Forces Europe

Distribution List (Con't)

Defense Documentation Center

Defense, Research and Engineering

Destroyer Development Group

Environmental Prediction Research Facility

Fleet Air - Azores

Fleet Air - Caribbean

Fleet Air - Keflavik

Fleet Air - Mediterranean

Fleet Air - Western Pacific

Fleet Air - Western Pacific Detachment Cubi Pt.

Fleet Air - Western Pacific Detachment Misawa

Fleet Air Wings - Atlantic

Fleet Air Wings - Pacific

Fleet Antisubmarine Warfare School

Fleet Area Control and Surveillance Facility

Fleet ASW School

Fleet Numerical Weather Central

Fleet Ocean Surveillance Information Facility

Fleet Training Group

Fleet Training Group Charleston, Norfolk, Pearl Harbor, San Diego and Western Pacific

Fleet Weather Central Norfolk, Rota

Fleet Weather Facility Jacksonville

General Dynamics

General Electric Co.

General Electric Co. Ocean Science Lab.

General Motors Corp.

Gulf Universities Research Consortium

Hawaii Inst. of Geophysics

Helicopter Antisubmarine Squadron 1, 2, 3, 4, 5, 6, 7, 8, 10, 11, 15, 74, 75, 84 and 85

Helicopter Antisubmarine Squadron, Light 30, 31, 32, 33 and 35

Helicopter Antisubmarine Wing One

Honeywell, Inc.

Distribution List (Con't)

Hydrospace Challenger, Incorporated

Interstate Electronics Corporation

Johns Hopkins Univ.

Kappa Systems, Inc.

Lulejian & Assoc., Inc.

Marine Physical Lab.

Mechanics Research, Inc.

Meterology International, Incorporated

NATO SACLANT Antisubmarine Warfare Research Centre

Naval Air Development Center - 3 Copies

Naval Air Force - Atlantic Fleet, Pacific Fleet

Naval Air Systems Command 2 Copies

Naval Coastal Systems Lab. - Port Hueneme, Calif., Panama City, Florida

Naval Electronic Systems Command

Naval Facilities Engineering Command

Naval Intelligence Support Center

Naval Ocean Surveillance Information Center

Naval Oceanographic Office - 5 Copies

Naval Ordnance Lab.

Naval Postgraduate School

Naval Research Lab. 3 Copies

Naval Sea Systems Command

Naval Ship Research and Development Center 2 Copies

Naval Surface Weapons Center

Naval Undersea Center 4 Copies

Naval Underwater Systems Center - 2 Copies

Naval War College

Naval Weather Service Command

Ocean Data Systems, Inc.

Oceanographer of the Navy

Distribution List (Con't)

Oceanographic Detachment 104, 105, 106, 108, 109, 114 and 115

Oceanographic Development Squadron 8

Oceanographic Systems, Atlantic, Pacific

Office of Naval Research 15 Copies

Office of Naval Research Boston Branch Office, Chicago Branch Office and Pasadena Branch Office

Operational Test and Evaluation Detachment, New London

Operational Test and Evaluation Force, Norfolk, Pacific

Operational Test and Evaluation Force Component Activity, Moffett Field

Patrol Squadron Detachment, Lajes, Rota and Sigonella

Patrol Squadron 1, 4, 5, 6, 8, 9, 10, 11, 16, 17, 19, 22, 23, 24, 26, 30, 31, 40, 44, 45, 46, 47, 48, 49, 50, 56, 60, 62, 64, 65, 66, 67, 68, 69, 90, 91, 92 and 94

Patrol Wing 1, 2 and 11

Patrol Wing 1 - Detachment Agana, Cubi Pt, Iwakuni and Naha

Patrol Wings Atlantic, Pacific

Patrol Wings Pacific Detachment Adak

Pennsylvania State Univ.

Raff Associates, Inc.

Raytheon, Inc.

Reserve Patrol Wing, Atlantic, Pacific

Rockwell International Corporation

Sanders Associates

Santa Barbara Associates

Science Applications, Incorporated

Scripps Institution of Oceanography

Sea Based Air ASW/ Commander Sea Control Group One

Singer Simulation Products Division

Sperry Rand Corporation

Distribution List (Con't)

Submarine Development Group 1, 2

Submarine Development Group 1 - Detachment, Mare Island

Submarine Flotilla 8

Submarine Force Atlantic Fleet

Submarine Force Atlantic Fleet Rep.

Submarine Group 2, 5, 6, 7 and 8

Submarine Squadron 1, 2, 3, 4, 6, 10, 12, 14, 15, 16 and 18

Submarine Squadron 15, Rep. Pearl Harbor

Systems Applications, Incorporated

Tetra-Tech, Inc.

Texas A & M University

Texas Instruments, Inc.

Tracor, Inc.

Training Command, Atlantic Fleet, Pacific Fleet

TRW Systems - 2 Copies

U. S. Coast Guard

U. S. Naval Academy

Underwater Systems, Incorporated

University of Miami

Vitro Laboratories

Western Electric Co.

Westinghouse Electric Corporation

Woods Hole Oceanographic Institution

Xonics, Inc.

DEPARTMENT OF THE NAVY
OFFICE OF NAVAL RESEARCH
875 NORTH RANDOLPH STREET
SUITE 1425
ARLINGTON VA 22203-1995

IN REPLY REFER TO:

5510/1
Ser 321OA/011/06
31 Jan 06

MEMORANDUM FOR DISTRIBUTION LIST

Subj: DECLASSIFICATION OF LONG RANGE ACOUSTIC PROPAGATION PROJECT (LRAPP) DOCUMENTS

Ref: (a) SECNAVINST 5510.36

Encl: (1) List of DECLASSIFIED LRAPP Documents

1. In accordance with reference (a), a declassification review has been conducted on a number of classified LRAPP documents.

2. The LRAPP documents listed in enclosure (1) have been downgraded to UNCLASSIFIED and have been approved for public release. These documents should be remarked as follows:

   Classification changed to UNCLASSIFIED by authority of the Chief of Naval Operations (N772) letter N772A/6U875630, 20 January 2006.

   DISTRIBUTION STATEMENT A: Approved for Public Release; Distribution is unlimited.

3. Questions may be directed to the undersigned on (703) 696-4619, DSN 426-4619.

BRIAN LINK
By direction

Subj: DECLASSIFICATION OF LONG RANGE ACOUSTIC PROPAGATION PROJECT (LRAPP) DOCUMENTS

DISTRIBUTION LIST:

NAVOCEANO (Code N121LC – Jaime Ratliff)
NRL Washington (Code 5596.3 – Mary Templeman)
PEO LMW Det San Diego (PMS 181)
DTIC-OCQ (Larry Downing)
ARL, U of Texas
Blue Sea Corporation (Dr.Roy Gaul)
ONR 32B (CAPT Paul Stewart)
ONR 321OA (Dr. Ellen Livingston)
APL, U of Washington
APL, Johns Hopkins University
ARL, Penn State University
MPL of Scripps Institution of Oceanography
WHOI
NAVSEA
NAVAIR
NUWC
SAIC

Declassified LRAPP Documents

Report Number	Personal Author	Title	Publication Source (Originator)	Pub. Date	Current Availability	Class.
Unavailable	Beam, J. P., et al.	LONG-RANGE ACOUSTIC PROPAGATION LOSS MEASUREMENTS OF PROJECT TRANSLANT I IN THE ATLANTIC OCEAN EAST OF BERMUDA	Naval Underwater Systems Center	740612	ADC001521	U
Unavailable	Cornyn, J. J., et al.	AMBIENT-NOISE PREDICTION. VOLUME 2. MODEL EVALUATION WITH IOMEDEX DATA	Naval Research Laboratory	740701	AD0530983	U
Unavailable	Unavailable	COHERENCE OF HARMONICALLY RELATED CW SIGNALS	Naval Underwater Systems Center	740722	ADB181912	U
Unavailable	Banchero, L. A., et al.	IOMEDEX SOUND VELOCITY ANALYSIS AND ENVIRONMENTAL DATA SUMMARY	Naval Oceanographic Office	740801	ADC000419	U
3810	Unavailable	CONSTRUCTION AND CALIBRATION OF USRD TYPE F58 VIBROSEIS MONITORING HYDROPHONES SERIALS 1 THROUGH 7	Naval Research Laboratory	741002	ND	U
ARL-TM-73-11; ARL-TM-73-12	Ellis, G. E., et al.	ARL PRELIMINARY DATA ANALYSIS FROM ACODAC SYSTEM; ANALYSIS OF THE BLAKE TEST ACODAC DATA	University of Texas, Applied Research Laboratories	741015	ADA001738; ND	U
Unavailable	Mitchell, S. K., et al.	QUALITY CONTROL ANALYSIS OF SUS PROCESSING FROM ACODAC DATA	University of Texas, Applied Research Laboratories	741015	ADB000283	U
Unavailable	Unavailable	MEDEX PROCESSING SYSTEM. VOLUME II. SOFTWARE	Bunker-Ramo Corp. Electronic Systems Division	741021	ADB000363	U
Unavailable	Spofford, C. W.	FACT MODEL. VOLUME I	Maury Center for Ocean Science	741101	ADA078581	U
Unavailable	Bucca, P. J., et al.	SOUND VELOCITY STRUCTURE OF THE LABRADOR SEA, IRMINGER SEA, AND BAFFIN BAY DURING THE NORLANT-72 EXERCISE	Naval Oceanographic Office	741101	ADC000461	U
Unavailable	Anderson, V. C.	VERTICAL DIRECTIONALITY OF NOISE AND SIGNAL TRANSMISSIONS DURING OPERATION CHURCH ANCHOR	Scripps Institution of Oceanography Marine Physical Laboratory	741115	ADA011110	U
Unavailable	Baker, C. L., et al.	FACT MODEL. VOLUME II	Office of Naval Research	741201	ADA078539	U
ARL-TR-74-53	Anderson, A. L.	CHURCH ANCHOR EXPLOSIVE SOURCE (SUS) PROPAGATION MEASUREMENTS (U)	University of Texas, Applied Research Laboratories	741201	ADC002497; ND	U
MCR106	Cherkis, N. Z., et al.	THE NEAT 2 EXPERIMENT VOL 1 (U)	Maury Center for Ocean Science	741201	NS; ND	U
MCR107	Cherkis, N. Z., et al.	THE NEAT 2 EXPERIMENT VOL 2 - APPENDICES (U)	Maury Center for Ocean Science	741201	NS; ND	U
Unavailable	Mahler, J., et al.	INTERIM SHIPPING DISTRIBUTION	Tetra, Tech, BB&N, & PSI	741217	ND	U
75-9M7-VERAY-R1	Jones, C. H.	LRAPP VERTICAL ARRAY- PHASE IV	Westinghouse Electric Corp.	750113	ADA008427; ND	U
AESD-TN-75-01	Spofford, C. W.	ACOUSTIC AREA ASSESSMENT	Office of Naval Research	750201	ADA090109; ND	U